Universiteit Utrecht

MSc Thesis

Wave-to-wave variability of skewness and asymmetry in the cross-shore:

A combined laboratory and modelling study

Math van Soest
4105664

Supervisor: Prof. dr. Gerben Ruessink
2nd Supervisor: Dr. Timothy Price

Date: November 28, 2020

Picture front page: Breaking waves at J-Bay, South Africa

Abstract

Reducing depths drive wave shapes to deform from nearly sinusoidal to non-linear, in the form of skewness and asymmetry. This non-linearity is reflected in the induced orbital velocity, which has strong implications for wave driven sediment transport. Commonly, non-linearity is calculated over a total time series comprising numerous waves or modelled using parameterisations (such as the ones founded on the Ursell-number) which are based on local short wave height and period, as well as water depth. These approaches neglect the potentially large wave-to-wave variability in skewness and asymmetry related to the grouped structure of the incident waves and the resulting presence of infragravity waves. The aim of this study is to analyse the wave-to-wave variability in the development of skewness and asymmetry in the cross-shore direction, on a steep and gentle slope, with an emphasis on the role of infragravity waves, by means of a data model approach. A total of three experimental settings from the GLOBEX dataset (Ruessink et al., 2013), containing high resolution data on the propagation of bichromatic waves over a gentle sloping bed (1:80), was analysed. The same three boundary wave conditions were modelled over a steep sloping beach (1:10), using numerical model SWASH. Both the laboratory and modelled data were analysed using an individual wave tracking algorithm developed for this study, capable of identifying the development of skewness, asymmetry, wave height, period, local depth and Ursell-number. Wave-to-wave variability was observed to be generally larger on a gentle bed slope, and explicitly in the inner surf zone ($Sk_{i,range}$ & $As_{i,range} \approx 1.6$). On a steep bed slope, the largest wave to wave variability was found in the outer breaking zone ($Sk_{i,range}$ & $As_{i,range} \approx 0.6$), and reduced in the inner surf zone. Through analysis of the relation between the Ursell-number and *Sk* and *As*, it is concluded that variability in short wave characteristics (e.g. wave height) determines wave-to-wave variability in the offshore and shoaling zone. At locations where infragravity wave height to depth ratio was large (inner surf zone, on a gentle bed), wave-to-wave variability in non-linearity was found to increase. Though further research into other complex hydrodynamic processes in the inner surf zone is suggested, infragravity waves are thought to impact wave-to-wave variability in skewness and asymmetry.

Acknowledgements

The process of writing a MSc thesis is commonly perceived as a lonely process. I embarked on this endeavour in February of 2020. Just a month in, the world was forced to a hold by the consequences of a pandemic outbreak. The norm was, and still is, to work from home as much as possible, making the process even more solitary. It is for this reason that I would like to express my appreciation to the people that have helped me throughout this period.

Firstly, great gratitude goes out to my supervisor Gerben Ruessink. Through various video calls he was able to communicate his absolute expertise within the field of research, provide meaningful feedback and guide me academically when I felt like I was freewheeling.

I want to thank Anouk de Bakker for taking a very proactive role in assisting me with the struggles of modelling and for suggesting me the intern position at Deltares which I will be taking after finishing this research.

I would like to express my great appreciation to my parents: René van Soest and Mariëlle Janssen, who have supported me throughout my educational quest which has ultimately landed me in the field of physical geography.

Finally, I want to thank my girlfriend Sara Spaargaren, who was of great mental support and who always kept me good company.

Table of Contents

1. Introduction

As wind blows across open waters, waves are created. These can range from a couple of centimetres to more than ten metres in height. In deep open waters these follow fairly linear (sinusoidal) patterns. However, as waves propagate closer to shore, their shape starts to deform. This transformation to non-sinusoidal wave shape is widely regarded as one of the key drivers of morphological change of wave-dominated coasts, as a consequence of induced sediment transport (Ruessink et al., 2012; Davies & Li, 1997). Insight in these complex hydrodynamic processes allows for a better understanding and predictability of the morphology of coastal systems.

The wave shape in deep water, where no interaction with the bed is taking place, is sinusoidal. When waves travel closer to shore and depths decrease both their surface form and orbital water motion become increasingly non-linear. Firstly, as a result of interaction with the bed, the process of shoaling is initiated. This is characterized by waveshapes consisting of sharp crests and broad, flat troughs (Fig. 1A). This form of non-linearity is commonly regarded as horizontal asymmetry or skewness (Doering & Bowen, 1995). Asymmetry occurs when waves reach even shallower depths and wave breaking is induced, resulting in an even steeper wave face and a gentle sloping rear face, commonly referred to as a sawtooth pattern, or vertical asymmetry (Fig. 1B; Elgar, 1987). The skewed and asymmetric wave shapes are reflected in their near-bed induced orbital velocities, generally generating onshore sediment transport. Consequently, the development of wave non-linearity is strongly connected to morphological recovery of beaches, after erosional effects of storms. Thus, these processes have been studied extensively.

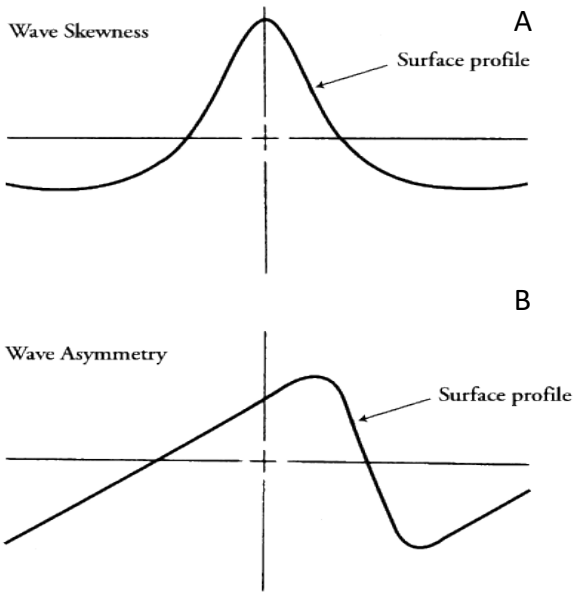

Figure 1: Schematic Visualistation of skewed (a) and asymmetric wave (b)

With rising sea-levels as a result of climate change, there is an increasing demand for correct modelling of the geomorphological behaviour of our coastal systems. The implications of skewness and asymmetry on onshore sediment transport, show that an accurate description of non-linear development is crucial in correct modelling. Despite the introduction of deterministic waves models that are capable of providing this accurate description, these are too computationally demanding to model morphological change on timescales of days, weeks and even years (Ruessink et al., 2012). In order to minimize computation time, parametrisations that correctly estimate the cross-shore development of non-linearity are needed. Currently, the parameterisations of skewness and asymmetry are based on local wave statistical parameters, such as wave height and length combined with

water depth (Rocha et al., 2017). With regards to wave height, single statistical time-averaged parameters such as the RMS (root mean square) wave height, significant wave height or maximum wave height are used for geomorphological modelling. However, when using such bulk estimates, individual wave variability is lost. In reality, individual waves from the same wavefield can differ height and length (Bretschneider, 1959), hence in skewness and asymmetry. Not taking wave-to-wave variability in non-linearity into account can lead to discrepancies between modelled and actual coastal morphology.

Abdelrahman and Thornton (1987) showed that local variations in mean water level, as induced by infragravity waves, alter short wave characteristics such as amplitude and wavelength. Infragravity waves are long period waves (25 – 250 seconds) that develop as a consequence of the presence of short-wave groups; the superposition between two wave trains of very similar wave lengths or frequency can amplify when waves are in phase and dampen when out of phase, creating wave groups or trains (Longuet-Higgins and Stewart, 1962; Brown, 1999). As a result of non-linear interactions (second-order Stokes), the short waves form a minor rise and depression in the mean water level at the wave group length. This can be thought of as a wave itself, that is 180-degrees out of phase with the wave groups (Fig. 2). Infragravity waves, similar to short waves, have been found to undergo the processes of shoaling and breaking too, meaning that the water-level offset they induce, increases in the shoreward direction towards their breaking point (Battjes et al., 2004). This process is more pronounced in the case of low sloping beaches, when compared to steep sloping beaches (De Bakker et al., 2016). By studying the development in celerity of individual waves, Tissier et al. (2015) found that the wave-to-wave variability in celerity increases when waves enter the surf zone as a result of infragravity waves. For this reason, it is expected that non-linearity of individual waveshape shows an increase in variability in the cross-shore direction, as a consequence of differences in short wave characteristics and the mean water level off-set generated by infragravity waves. In addition, it is expected that a gentle beach slope can enhance non-linear variability in the cross-shore direction, as a result of the increased water-level offset from shoaling of infragravity waves, when compared to a steeper beach slope (De Bakker et al., 2016). Whether this is indeed the case has not been researched before. This present study aims to analyse the wave-to-wave variability in the development of skewness and asymmetry in the cross-shore direction, on a steep and gentle slope, with an emphasis on the role of infragravity waves.

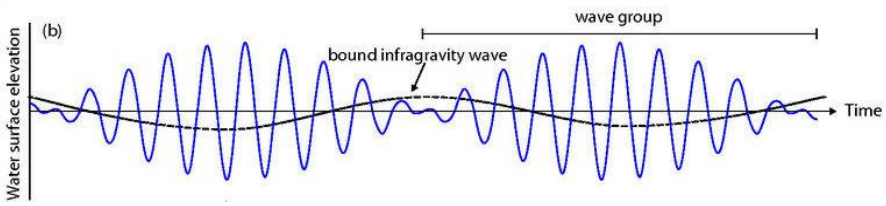

Figure 2: Schematic definition of bound infragravity wave

This has been achieved by means of a data and modelling study, focussed on tracking individual waves in the cross-shore direction over a gentle and steep sloping beach and by studying the development of their non-linearity. This provided insight in the development of the range of variability in both skewness and asymmetry. The findings were analysed and related to the characteristics of infragravity waves. In order to accurately track individual waves a high-resolution dataset (both in space and time) of free surface elevation was required. The GLOBEX laboratory experiment as conducted and described by Ruessink et al. (2013), was an adequate match. Bichromatic waves were forced over a low sloping (1:80) beach and the water level was measured by 191 gauges at 128 Hz. These results were then compared to numerical data retrieved from the SWASH-model. This is a general-purpose numerical tool for simulating waves (TU Delft: SWASH, n.d.), which was used to recreate the physical experiment, in order to validate the modelled data. Ultimately, SWASH was utilised to model waves propagating over a steeper beach slope (1:10).

This work is a complete and thorough description of the executed research and its outcomes. It starts with a literature review (Chapter 2) where relevant concepts and theories are elaborated upon, followed by a problem definition and research focus. Next, the methodology applied for conducting this study is thoroughly discussed (Chapter 3), firstly, focussing on the GLOBEX experimental set up; secondly, on how its data was analysed; and thirdly, explaining how the numerical SWASH model was set-up and validated. Results of the development of individual wave non-linearity in the cross-shore are visualised and quantitatively discussed (Chapter 4). The results and their implications are then thoroughly interpreted and discussed (Chapter 5). Finally, the conclusions for this research are summed up (Chapter 6).

2. Literature Review

2.1 Water Depth Regimes and Development of Non-Linearity

In order to describe the evolution of ocean waves over beaches, three depth zones are defined. The water particle motion, as induced underneath a travelling wave, follows an almost circular pattern. Under the wave crest, water particles flow in the traveling direction of the wave, under the through they flow against the traveling direction of the wave. The velocity wave induced particle movement reduces with depth (Fig. 3). Deep water is defined by depth extending deep enough that the water motion induced by the wave does not interact with the bed. This is the case for $h / L > 0.5$ where h is depth in meters and L is wavelength in meters (Masselink and Hughes, 2003; van Rijn, 1990).

When waves propagate further onto beaches, intermediate water depth is reached. This is defined as $h / L < 0.5$. At this point water motion as induced by the wave is interacting with the bed (Fig. 3). The water particle motion close to the bed is now more elliptical, allowing horizontal particle transport. Also, at this point the wave starts to deform, increasing in amplitude and shortening its length, commonly referred to as shoaling.

In even shallower water the wave induced water motion becomes even more horizontal. The shallow water zone is defined by $h / L < 0.05$. It is within this water depth regime that waves break. Four different types of wave breaking can be distinguished: spilling, plunging, collapsing and surging (Galvin Jr., 1968). The distinction between breaker types has been investigated by Battjes (1975). He developed the *surf similarity*-parameter, which distinguishes between breaker types. It was found that this depends on the offshore steepness of the waves and on the bed slope. In this same study it is noted that wave breaking occurs under a certain depth to wave height ratio. This is noted as $\gamma_b = H_b/d_b$, where H_b represents breaking wave height and d_b represents the breaking depth. It was found that $\gamma_b \approx 0.8$, although values between $\gamma_b = 0.4$ and well over $\gamma_b > 1$ have been reported too.

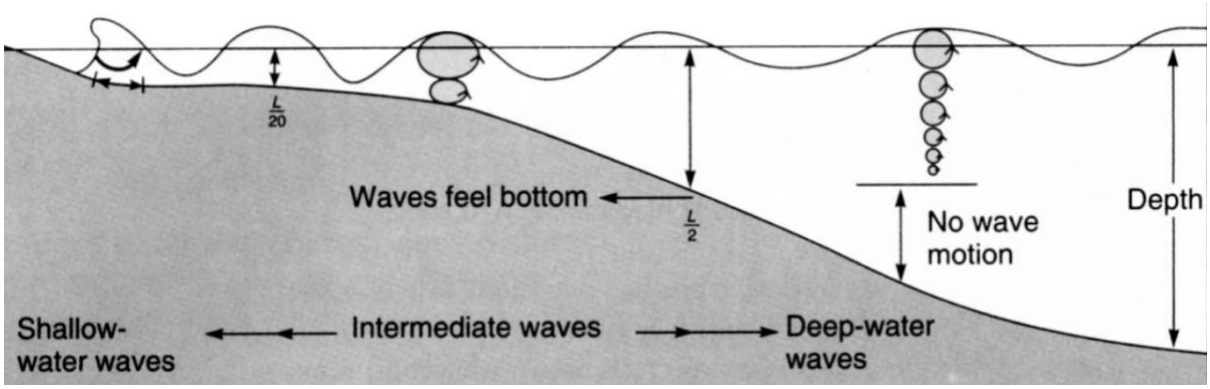

Figure 3: Cross-shore wave shape development

When waves propagate from deep into shallower water, meaning that H/h becomes small, linear wave theory is no longer valid. Due to shoaling, wave faces become steeper. For this, non-linear wave theory plays an important role. The most renowned theory stems from 1847 and was introduced by Stokes, commonly known as Stokes' Wave Theory. Various kinds of expansions have been introduced over the years (Fig. 4). However, in shallow water waves become non-linear to such an extent, that even these forms of non-linear theory do not hold. Guza and Thornton (1980) demonstrated that with a slope of 1.3° (or ≅ 1:77), linear shoaling theory results in a 20% error in predicting wave height, from 10 m to 3 m depth. This error increases from 3 m depth shoreward. This underlines the importance of developing a thorough understanding of nonlinear effects in near shore hydrodynamics.

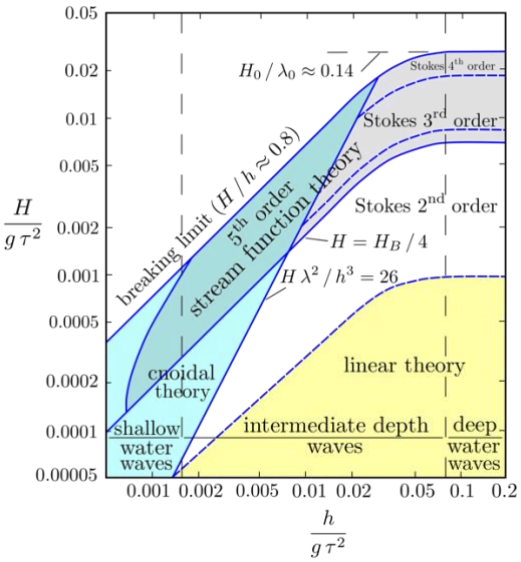

Figure 4: Various kinds of non-linear wave theory

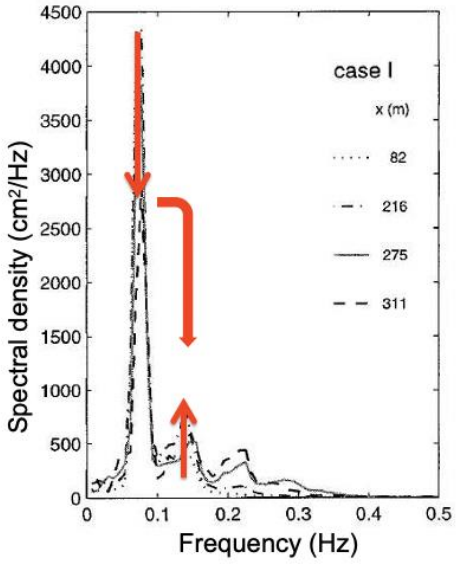

Figure 5: Non-linear sum interactions visualised in a frequency distribution

2.2 Skewness and Asymmetry

2.2.1 Wave Shape

As a result of nonlinear effects, waves shapes that were nearly sinusoidal in deep water, transform as they propagate over beaches perpendicular to the coast. Through the amplification of higher harmonics (multiples of the primary peak frequency) as depth reduces, throughs are lengthened and crests are shortened but elevated, also known as vertical asymmetry or skewness. As depths reduce further and wave breaking is induced, the wave crest starts to pitch forward, causing a sawtooth like pattern. This is known as asymmetry, or horizontal asymmetry (Sorensen, 2005).

Both shape transformations are a consequence of the nonlinear triad interactions, where energy is transferred between three wave components. Initially, from pairs of wave components (frequencies f_1 and f_2) near the dominant spectral peak f_p, energy is transferred

to higher frequencies by the sum interactions ($f_1 + f_2 = f_3$). Typically, the frequency for the primary, secondary and peak wave components are close ($f_1 \approx f_2 \approx f_p$), and the third frequency, to which energy is transferred, is a higher harmonic ($f_3 = 2f_p$; Elgar & Guza, 1985). This is visualised in Figure 5.

Skewness and asymmetry are defined by asymmetry on the vertical and horizontal axis, as schematized in Figure 6 by the vertical solid and horizontal dashed line. The horizontal axis represents the mean sea water level. For linear waves the ratio between wave height (*H*) and the amplitude (a_c), is $a_c / H = 0.5$. When waves are skewed as a result of shoaling, the ratio increases to ≈ 0.75. Around this point wave breaking is induced and waves start pitching forward, altering the ratio between *1* and *2* (Sorensen, 2005).

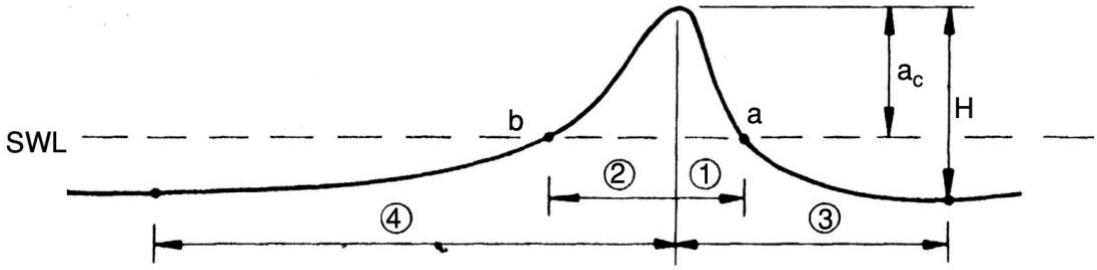

Figure 6: Non-linear wave with symmetrical axes Sorenson (2005)

More commonly, skewness (*Sk,* Equation 1) is defined as a function of the free surface elevation (η) averaged over time (indicated by < … >). Asymmetry (*As,* Equation 2) is defined by taking the Hilbert transform (H) of the free surface elevation of η for the numerator. This provides the following formulations, as defined by Elgar et al. (1987):

$$Sk = \frac{<\eta^3>}{<\eta^2>^{3/2}} \qquad \text{eq. 1}$$

$$As = \frac{<H(\eta)^3>}{<\eta^2>^{3/2}} \qquad \text{eq. 2}$$

In sufficiently deep water, when waves are nearly sinusoidal, both skewness and asymmetry remain low ($Sk \approx 0$; $As \approx 0$). As waves propagate into shallower waters, while the process of shoaling is progressing wave become increasingly skewed, or vertically asymmetric ($Sk > 0$). When water depths decrease further and waves start pitching forward and eventually break, the skewness decreases ($Sk \approx 0$), while waves become increasingly asymmetric or horizontally asymmetric ($As < 0$). Note that for asymmetry, an increase in nonlinearity is signified by the number becoming more negative, whilst for skewness an increase in nonlinearity is signified by the number becoming more positive. Maximum values for skewness are in the order of $Sk_{max} \approx 1\ to\ 2$, for asymmetry these values are in the order of $-As_{max} \approx -1\ to\ -2$.

2.2.2 Induced flow and sediment transport

The implications of these parameters, on orbital velocity and consequently sediment transport, are the main reason for wave skewness and asymmetry being thoroughly researched. When a wave is skewed, the flow velocity it induces near the bed follows an orbital pattern of high flow velocities during a short period of time (underneath the crest) in the onshore direction, followed by low flow velocities in the offshore direction during a longer period of time (underneath the through). The high flow velocities stir the sand, resulting in larger concentrations of coarse sediment near the bed, known as bed load, which are in phase transported with the water flow in the onshore direction. When finer sediment is stirred, it reaches further from the bed (higher in the water column), also known as suspended sediment. Suspended sediment needs more time to settle down, creating a settling lag, and is consequently transported during the lower velocities directed offshore as induced by wave crest. However, as the total sediment concentrations are largest during the high onshore flow velocities, skewed waves transport sediment in the onshore direction. This mechanism was demonstrated in a laboratory experiment by (Ribberink et al., 2008).

Asymmetric waves are also known to induce onshore sediment transport. Just prior to and during the process of wave breaking, the sawtooth shape with steep faces and more gently sloping rear faces, generates strong flow velocity accelerations under the steep face, similar to skewed waves. However, as a result of more pronounced phase lag effects, the offshore flow underneath the through is capable of transporting a similar amount of sediment (Elgar et al., 1988). The induced onshore flow is capable of transporting just slightly more sediment. However, underneath asymmetric waves, in the surf zone, the sediment is stirred more vigorously when compared to skewed waves in the shoaling zone, leading to much greater sediment concentrations that are being suspended. For this reason, wave asymmetry is considered to have a larger influence on onshore sediment transport than wave skewness (Austin et al., 2009). This underlines the importance of investigating the development of wave shape asymmetry.

2.3 Ursell-number

Wave nonlinearity of skewness and asymmetry is often parametrised and based on local wave statistical parameters, such as wave height and length combined with water depth, of which the most renowned example is the Ursell number (Eq. 5). This is a dimensionless parameter introduced in 1953 by Fritz Ursell. It is defined by the following functions as defined by Doering & Bowen (1995); where *h* represents depth; a_w represents the amplitude of the wave as half of the wave height (*H*) and *k* represents the wave number as a function of the wave length (*L*).

$$a_w = 0.5\ H \qquad \text{Eq.3}$$

$$k = \frac{2\pi}{L} \qquad \text{Eq.4}$$

$$Ur = \frac{3}{4}\frac{a_w\ k}{(kh)^3} \qquad \text{Eq.5}$$

Doering and Bowen (1995) have related the Ursell-number to the development of orbital velocity skewness and asymmetry. This work has been elaborated by Ruessink et al. (2012). From 30.000+ field observations of flow velocity skewness and asymmetry it was established that the Ursell-number describes the variability in skewness and asymmetry well. The fitted relation as found by Ruessink et al. (2012) is visualised in Figure 7. According to these fits, when waves are (close to) sinusoidal, both skewness and asymmetry are low; correspondingly the Ursell-number is also low (Ur < 0.1). As depth decreases and the process of shoaling causes the waves to skew to a maximum level, asymmetry is still small (Ur ≈ 1). As the process of wave breaking is induced, asymmetry increases and skewness reduces back to zero (Sk ≈ 0, As < 0), Ur increases exponentially. Consequently, the Ursell-number represents the non-linearity in one single number (Doering & Bowen, 1995; Ruessink et al., 2012).

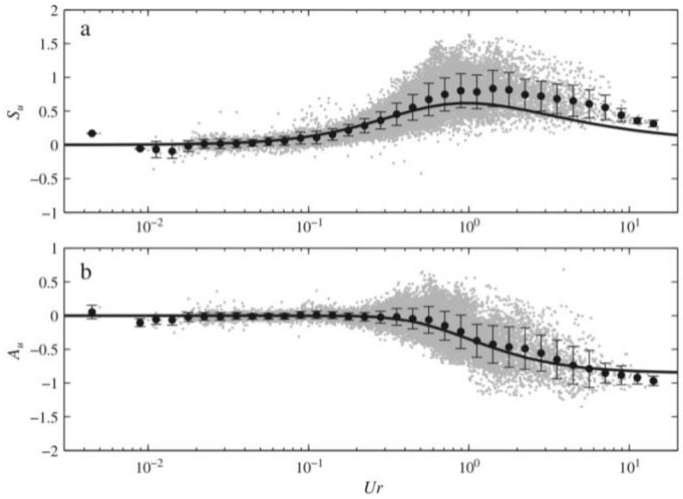

Figure 7: Relation between Ursell-number and Sk & As (Ruessink et al., 2012)

It should be noted that despite the use of such an extensive data set, there is much scatter that is not explained by these fits. Ruessink et al. (2012) appoint this to directional spread of wave propagation in the field. For this reason, the proposed fits have been criticised and improved by Rocha et al. (2017) and De Wit et al. (2019).

The first study critiques the parameterisations for nonlinearity as a function of Ursell as suggested by Ruessink et al. (2012) and suggests improvements. When comparing the modelled results against the parameterisation as suggested by Ruessink et al. (2012), clear under estimations are found. It should be noted that results from Rocha et al. (2017) are numerically modelled whereas those of Ruessink et al. (2012) are based on a large quantity of field data. When altering bed slope, varying relationships between *Ur* and non-linearity parameter *B* (combining skewness and asymmetry) are found. It was found that the underestimation correlates negatively with increasing wave height (e.g. larger underestimation for smaller wave height), and positively with bed slope, both visualised in Figure 8. It is also noted that skewness is mainly affected, asymmetry less so.

The latter study by De Wit et al. (2019) indicates that in deeper water, variability in wave shape non-linearity was well-explained by variability in local *Ur*. However, in shallower water, only part of the variability in skewness and asymmetry could be explained by the variability in Ursell. This indicates that some physical processes are not properly accounted for. Towards shallower depths, a rapid decrease of *Ur* is observed for breaking conditions. This decrease, caused by a reduction in wave amplitude, dominates *Ur*. For non-breaking conditions an increase in *Ur* is observed, caused by a reduction in depth. This causes significant scatter in *Sk* and *As* as a function of *Ur* at shallow locations. The increase in scatter in shallower water could be attributed to a combination of three main physical process: spatial variability in tidal currents, wave-breaking and the nonlinear energy transfer rate. Wave lengths were found to respecivelydecrease and increase with opposing and following tidal currents, causing a decrease in *Ur*. Also, it is noted that *Ur* does not properly account for non-linear energy transfer rates. The wave shape non-linearity reacts to changes in depth with some delay. By adapting the fits of *Ur* with values that correspond to an earlier stage of wave transformation through slightly increasing depth, a reduced variance from 0.09 to 0.08 was found for *Sk* (Fig. 9). This indicates an improvement of predicting non-linearity from *Ur*. (De Wit, 2019). In this study the effects of infragravity waves are not discussed. The larger values of *Ur* are produced in shallower depths, where the predicting capabilities of *Ur* with regards to *Sk* and *As* were found to be less accurate. Especially in these shallower locations infragravity waves can become a dominant factor (De Bakker et al., 2016).

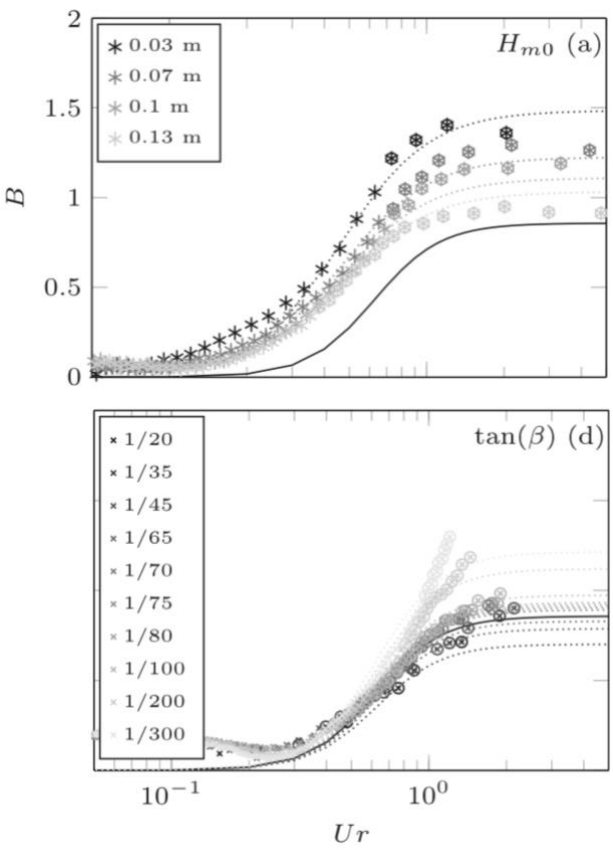

Figure 8: Nonlinearity parameter B calculated for runs with varying wave height and bed slope; solid line Ruessink fits, dashed lines fluctuating (a) H_{m0} and (d) bed slope fits (Rocha et al., 2017).

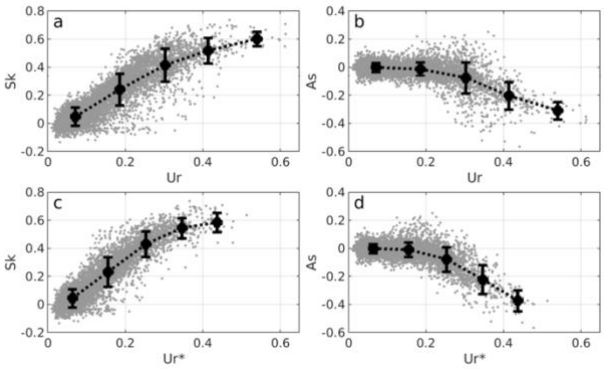

Figure 9: (a) Sk and (b) As as a function of local Ur. (c) Sk and (d) As of a function Ur∗ (with adjusted depth; De Wit et al., 2019)

2.5 Infragravity Waves

Besides the wind-generated “short” waves, lower frequency waves are present in oceanic waters. These waves are commonly known as infragravity waves. Typically, these are defined by wave frequencies between 0.004 and 0.04 Hz, whereas short-wave frequencies are defined between 0.04 and 1 Hz. At relatively low water depth, long-waves demonstrate wavelengths that stretch far longer than short waves, ranging from a few hundred meters to kilometres. Infragravity waves have been known to play a significant role in coastal hydrodynamics, sediment transport and various other coastal processes (Berntin et al., 2018). It is perceived that the presence of long waves can modify characteristics of short waves, such as amplitude and wavelength (Abdelrahman and Thornton, 1987), underlining the importance of considering these in this present study.

In 1949, Munk identified that the presence of short-wave groups is related to the lower frequency motions of run-up along the shoreline. Longuet-Higgins and Stewart (1962) theoretically esthablished that short waves induce a long wave that is bound to the incident wave group. They developed and applied their concept of radiation stress to a one-dimensional bichromatic wave-field. This is a wave signal that travels onshore with two specific frequencies. The superposition between two wave trains of very similar wave lengths and / or frequencies can amplify when waves are in phase and dampen when out of phase, creating an offset in the mean water level. The short waves form a minor rise under the smaller waves of a group and depression in the mean water level under the larger waves of a group (Brown, 1999). This can be thought of as a wave itself that is 180-degrees out of phase with the wave groups and has the same wavelength as the length of the short wave group. This phenomenon is known as bound long-waves. This is visualised in Figure 2.

Another driver of infragravity wave energy is the variation of breakpoint. This was identified by Symonds et al. (1982). Larger short waves within the group tend to break at larger depths, further offshore when compared to smaller short waves. This process is visualised in Figure 10. This breakpoint mechanism acts a sort of wave maker and generates both a free long wave obliquely incident towards the shore, also known as the release of the bound infragravity wave, and a free long wave directed offshore. The shoreward free wave is then also reflected in the seaward direction. The interaction between the incident and the reflected infragravity waves generates a standing (or stationary) wave pattern with nodes and antinodes (Bertin et al., 2018).

It was found by Basco and Yamashita (1986) that the width of the breaking zone is dependent on the previously discussed *surf similarity*-parameter as found by Battjes (1975). This suggests that it is, amongst others, dependent on bed slope. On a steeper bed slope the cross-shore width of the breaker zone is smaller, as the location where the largest and smallest waves break is narrow. On a steeper bed slope the breaker zone is wider.

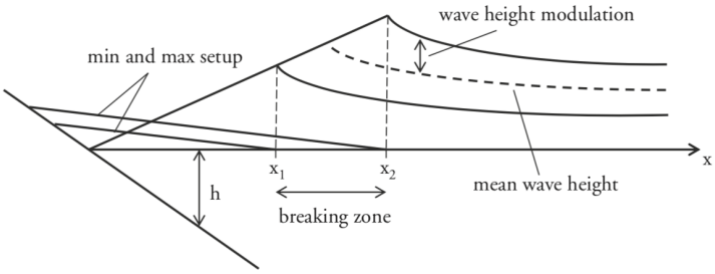

Figure 10: Wave height modulation as a consequence of infragravity waves (Brentin et al., 2018)

Within the inner surf and swash zones infragravity waves can be more energetic when compared to short (wind) waves. It was found that energy transfered from short waves makes these lower frequency waves more energetic. Similar to the previously discussed sum interactions, where short waves transfer energy to their higher harmonics, short waves also transfer energy to infragravity waves through difference interactions. These are defined as: $f_1 - f_2 = f_3$ (Herbers et al., 1994). Through these interactions, infragravity waves have been found to undergo the process of shoaling, through which their wave height increases. This behaviour can be seen as progressive. With regards to the development of nonlinearity of infragravity waves De Bakker et al. (2015) applied a bispectral analysis to identify these nonlinear energy transfers that involve infragravity frequencies. Within the shoaling zone, nonlinear interactions mainly result in an energy transfer from the spectral peak to its higher harmonics by sum interactions. Infragravity waves gain energy by difference interactions. Shoreward of the surf zone, little to no energy remaims from the short waves. Here, the nonlinear interactions are dominated by these infragravity frequencies. Consequently, as most short waves have dissipated energy through breaking, the infragravity waves from the dominant source of energy in the inner surf zone. This was found to be particularly true during high energy conditions (Guza & Thornton, 1982; Ruessink et al., 1998).

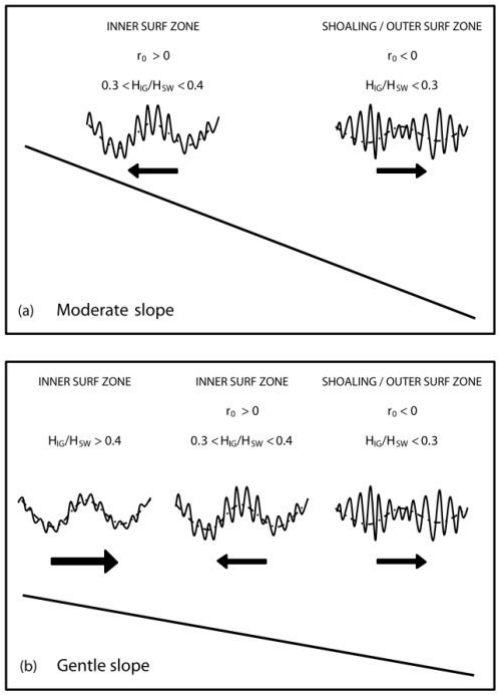

Figure 11: Schematic effects of bed slope on the modulation of short waves (De Bakker et al., 2016)

Abdelrahman and Thornton (1987) investigated the ways in which infragravity waves can modulate short wave characteristics. Firstly, they stated analytically that as a consequence of the slowly varying depth, as induced standing long waves, this modulates the amplitude, wavenumber (which includes wave length) and propagation direction of short waves. Following a field study, it was identified that in deeper water a negative correlation

exists between the incident short wave envelope and the infragravity motion (indicating a phase difference of 180°). In the surf zone, as infragravity waves are released, this correlation is positive which confirms the analytically demonstrated short wave modulation of infragravity waves.

De Bakker et al. (2016) found that the energetic dominance of infragravity waves in the inner surf zone was more pronounced on low sloping beaches, when compared to steep sloping beaches. This is conceptually visualised in Figure 11. Through the analyses of two field data sets, it was found that on a moderately sloping beach (1:35), infragravity wave height was relatively small when compared to the sea swell waves ($H_{ig} / H_{sw} < 0.4$), despite offshore wave conditions being energetic with heights reaching close to 5 m. On the gentle sloping beach (1:80) it was found that infragravity waves were more energetic when compared to the sea swell waves ($H_{ig} / H_{sw} > 0.4$). This figure also shows the development of r_0. This parameter represents the correlation of the infragravity-wave orbital motion with the sea-swell wave envelope, similar to Abraham and Thornton (1987). When an infragravity wave is bound (offshore) the largest short waves (thus envelope) are found at the trough of the infragravity wave, indicated by a negative $r_0 < 0$. Closer to shore, where the bound wave is released, a positive correlation is found where the short wave envelope is largest at the crest of the infragravity wave, indicated by a positive $r_0 > 0$. Consequently, short waves are modulated by the infragravity waves. It is found that this effect is stronger on a gentle sloping beach, when compared to a moderately sloping beach. Also, it is hypothesized that this modulation on steep sloping beaches is small or even absent.

2.6 Problem Definition and Hypoptheses

Properties of individual waves can differ greatly. Around the 1950's, various distribution types were introduced for describing the variability in short wave height and length. Longuet-Higgins (1952) suggested that a Rayleigh distribution captures this variability in oceanic waters rather well. Such distributions emphasize that individual waves have unique properties with regards to height and length, with consequently varying celerity. Tissier et al. (2015) found that the wave-to-wave variability of celerity, is large in a natural surf zone, with faster bores overtaking slower ones and sometimes merging.

Rocha et al. (2017) investigated the influence of offshore wave conditions and beach slope on the development of wave non-linearity. Wave conditions; such as offshore wave height (H_{m0}), peak period (T_p), spectral bandwidth (γ) and bed slope ($tan(\beta)$) were varied and simulated using the SERR1D model. It was found that the development and maxima of wave non-linearities, as expressed by skewness and asymmetry, are dependent on those wave conditions. Smaller offshore H_{m0} (for the same T_p) and greater offshore T_p (for the same H_{m0}) lead to greater maximum value of non-linearity. In addition, a decreasing bed slope leads to larger maximum skewness and similar maximum asymmetry but is initiated at a greater depth (Fig. 12h). These findings are visualised in Figure 12. This suggests that non-linearity of individual waves with different characteristics, or when propagating over a different bed

slope, will develop differently. Despite these modelled results being based on varying bulk estimates of the offshore wave conditions, these finding indicate that when characteristics of individual short waves differ, a varying development in non-linearity is observed.

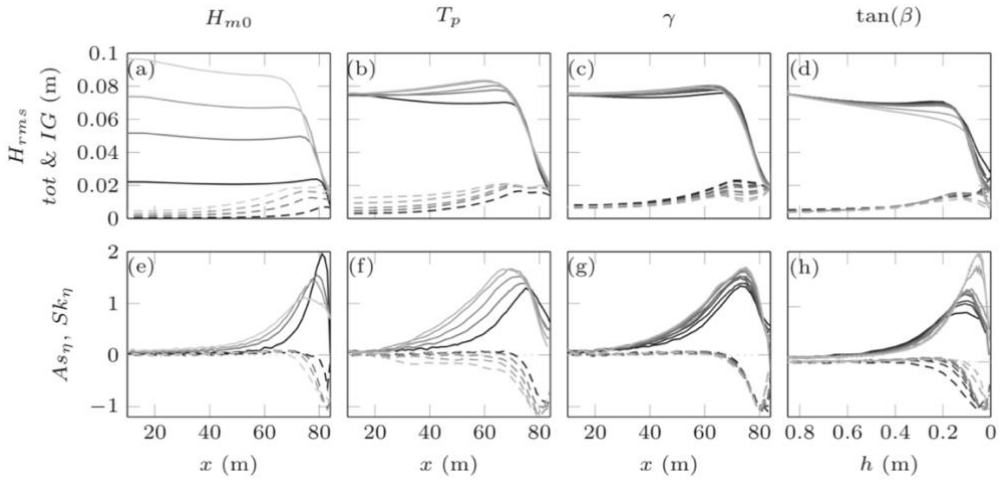

Figure 12: Cross-shore evolution of Hrms (solid lines – total; dashed lines IG waves only), Skη and Asη as a function of (a)/(e) offshore wave height, (b)/(f) offshore peak period, (c)/(g) offshore spectral bandwidth, (d)/(h) beach slope (Rocha et al., 2017)

Tissier et al. (2015) analysed data from two high-resolution laboratory experiments, where bichromatic waves were forced over a constant sloping beach. Through an analysis of individual wave development from these laboratory experiments, it was found that variability in celerity increases within the surfzone. This variability was seen to relate to the presence of infragravity waves. When the standard deviation of individual wave celerity was plotted as a function of the mean value of $Hrms,lf\ /\ \bar{h}$ ($H_{rms,lf}$ = Root Mean Square Infragravity Wave Height , $\bar{h}$ = Depth), an approximately linear trend is found (Figure 13). This confirms that when the ratio of infragravity wave height over depth increases ($H_{rms,lf}/h \geq 0.15$), correspondingly an increase in the wave-to-wave variability in celerity is observed.

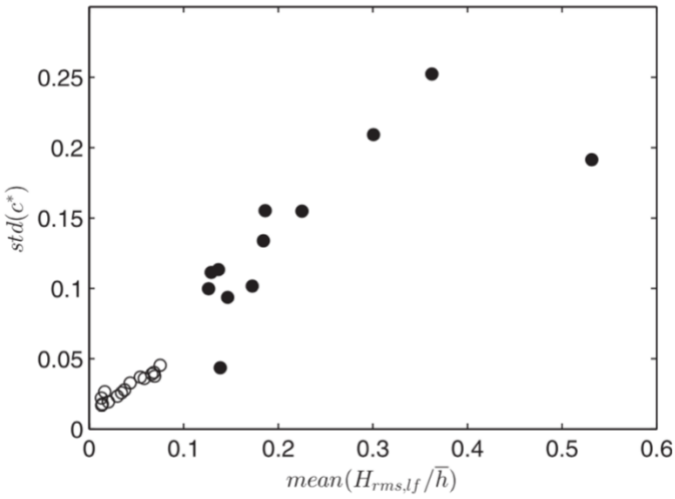

Figure 13: Standard deviation of individual celerity as function of the infragravity wave height over depth ratio (Tissier et al., 2015)

Findings by Rocha et al. (2017) implicate that when tracking individual short waves of varying characteristics (e.g. wave height) a variability in skewness and asymmetry is found. De Wit et al. (2019) observe that Ursell is capable of explaining variation of skewness and asymmetry, but less so in the inner surf zone, as a consequence of complex hydrodynamics. Findings by Tissier (2015) point out that, as a consequence of the infragravity induced mean water level off-set, the wave-to-wave variability in celerity increases in the inner surf zone. These observations combined have led to hypothesize that, regarding the cross-shore

development of individual waves, different short wave characteristics will drive wave-to-wave variability in skewness and asymmetry, in the offshore and shoaling zone. In the surf zone, it was expected that, similar to variability in celerity, an increase in wave-to-wave variability occurs when the infragravity wave height over depth ratio is large ($H_{rms,lf}/h \geq 0.15$). On a gentle bed slope this variability in non-linearity would be more pronounced, as the infragravity waves are more progressive, when compared to a steeper bed slope, based on findings of De Bakker et al. (2016) and Rocha et al. (2017). This has not been studied before.

2.7 Study Aim Research Questions

The aim of this study is to analyse the wave-to-wave variability in the development of skewness and asymmetry in the cross-shore direction, on a steep and gentle slope, with an emphasis on the role of infragravity waves. This is achieved by a modelling and data analysis study that involves tracking the non-linear development of individual waves. In order to achieve accurate wave tracking a high-resolution data set, both in space and time, containing free surface elevation of bichromatic waves (containing short and infragravity wave frequencies) propagating over a constant bed slope, was necessary. The GLOBEX data set, retrieved from a laboratory experiment, was an adequate fit. This dataset contains information on free surface elevation, measured by 190 gauges at 128 Hz, of bichromatic waves propagating over a low sloping beach; 1:80 m (Ruessink et al., 2013). Another data set containing information of a similar experiment of waves propagating over a steep sloping bed was needed for comparison. As no such data set exists the phase resolving SWASH-model has been utilised. This is a general-purpose numerical tool for simulating waves (TU Delft: SWASH, n.d.), which will be used to recreate the physical experiment to validate data retrieved from the numerical model. Ultimately, the model will be utilised to model waves propagating over a steeper beach slope (1:10).

An individual wave tracking algorithm was created, that traces waves through the cross-shore and calculates the development various characteristics, including non-linearity parameters skewness and asymmetry. Findings of this analysis will be presented and discussed in order to formulate coherent answers on the following research questions:

1. How does the wave-to-wave variability of skewness and asymmetry develop in the cross-shore direction?
2. What is the influence of the infragravity waves on wave-to-wave variability of non-linearity?
3. What is the influence of bed slope on the wave-to-wave variability of nonlinearity?

As a spin-off, the conventional ways of calculating skewness and asymmetry are compared to findings of the individual wave analysis. It is relevant to investigate whether this more detailed approach to wave non-linearity creates discrepancies, or whether it resembles the more traditional approach.

3. Methods

3.1 GLOBEX experiment

The laboratory experiment, examined in this study, was executed in the Scheldegoot flume at Deltares (Delft, Netherlands). The flume was 110 m long, 1 m wide and 1.2 m high. The experimental set-up is visualised in Figure 14. The bed started with a straight section that runs to 16.57 m (cross shore distance from the wave maker) and then went up following a gentle slope of 1:80. The mean shoreline was located at 84.57 m from the wave generator. This led to a still water depth of 0.85 above the plain section. The purpose of the GLOBEX laboratory experiment, was to investigate short wave and infragravity wave interaction (Ruessink et al., 2013). Within the flume, waves were generated using a piston-type wave maker, which possessed *Active Reflection Compensation,* allowing minimisation of reflection at the seaward boundary. This piston was capable of producing regular waves with a maximum height H of 0.4 m and irregular waves with a significant wave height H_s of 0.25 m.

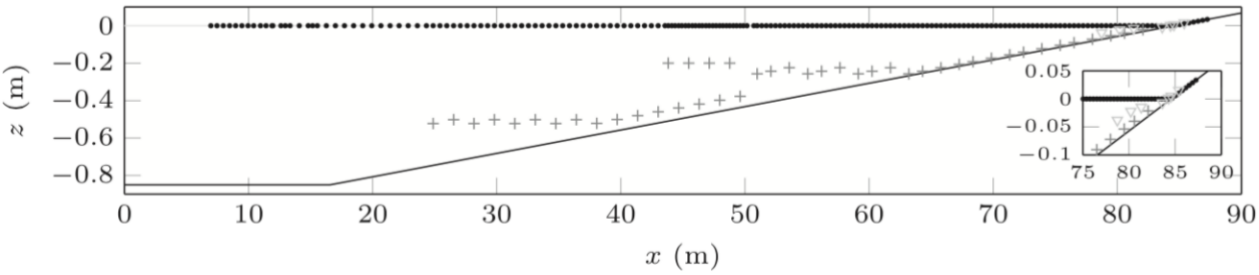

Figure 14: Experimental setup, with elevation z vs. crossshore distance x (both in meters). Dots represent the surface elevation gauges and plusses the velocity measurements (Ruessink et al., 2013)

Eight wave conditions were simulated, together compiling three series titled A, B and C. Series A consisted of random short waves, which resembled field conditions. Series C contained two single monochromatic wave cases in which groups do not exist. Series B comprised of three bichromatic wave cases, this research focusses on those three bichromatic experiment settings. All series were repeated ten different times with identical paddle motion and with instrument gauges placed at different positions. This led to 190 measurement locations of water surface elevation η at 128 Hz (Fig. 14). Each of the three B-series consisted of an effective time length of 24-minutes.

For the B series, wave conditions wee determined by two specific short wave frequencies. Consequently, this led to the presence of monochromatic infragravity waves in the experimental flume. The wave signal characteristics are presented in Table 1. The amplitudes corresponding both f_1 and f_2 frequencies were identical in B1 and B2. However, the frequencies of the primary components f1 and f2 varied such a way that the infragravity frequency f3 = f2 – f1 decreased from 0.067 to 0.042 Hz. Series B3 consisted of the same

frequencies as B2. However, the group modulations were enhanced by decreasing amplitude a_1 and increasing a_2. In all three series B cases the sum of both amplitudes equalled 0.1 m.

Table 1: Overview of waveconditions for GLOBEX B-series (Ruessink et al., 2013)

	a_1 (m)	a_2 (m)	f_1 (Hz)	f_1 (Hz)	**Remark**
B1	0.09	0.01	6/15	7/15	$1/f_3 = 15.0s$; $f_{mean} = 0.433$ Hz
B2	0.09	0.01	0.420	0.462	$1/f_3 = 23.8s$; $f_{mean} = 0.441$ Hz
B3	0.07	0.03	0.420	0.462	$1/f_3 = 23.8s$; $f_{mean} = 0.441$ Hz

As the analysis of individual waves will be linked to the presence of the infragravity waves, which are a consequence of the presence of the wave groups, it is important to note that in the GLOBEX experiment B series, the wave input was defined in such a way that wave groups consisted of an integer number of waves. In the case of B1, the difference between f_1 and f_2 was 1/15 Hz, or 0.0667 Hz (15.0 s). The primary wave frequency was set at 6/15 Hz, or 0.4 Hz, meaning that each wave group consisted of a total amount of 6 waves. In this case the wave period of the long (infragravity-) wave was 6 times the period of the primary wave frequency. For the B2 and B3 series, the difference between f_1 and f_2 is 0.042 Hz (23.8 s). The primary wave frequency was set at 0.42 Hz, meaning that each wave group consisted of a total of 10 waves. In this case the wave period of the long (infragravity-) wave was 10 times the period of the primary wave frequency.

3.2 Data Analysis

3.2.1 Detrending and filtering

Firstly, as a result of set-up and set-down the mean water levels increase as the waves shoal and break. This effect was to be taken away from the data and by subtracting the mean water level for each gauge, as averaged over the entire time series of the data set. This makes sure that the free surface elevation, averaged around 0.

Secondly, the free surface elevation data needed to distinguish between information on the high frequency (short) waves, and low frequency (long) waves. This was done using a bandpass filter. In the field, the high frequency band is typically set between 1 Hz and 0.05 Hz. The low frequency band is then set between 0.05 Hz and 0.005 Hz (Serverance, 1970). However, since this laboratory experiment was executed at smaller scale and the wave frequencies are known, it was possible to fine tune this. The high frequency band was set between 5 and 0.3 Hz. The low frequency band was set between 0.3 and 0.005 Hz. An example is shown in Figure 15. This approached proved to accurately divide the high and low wave frequencies.

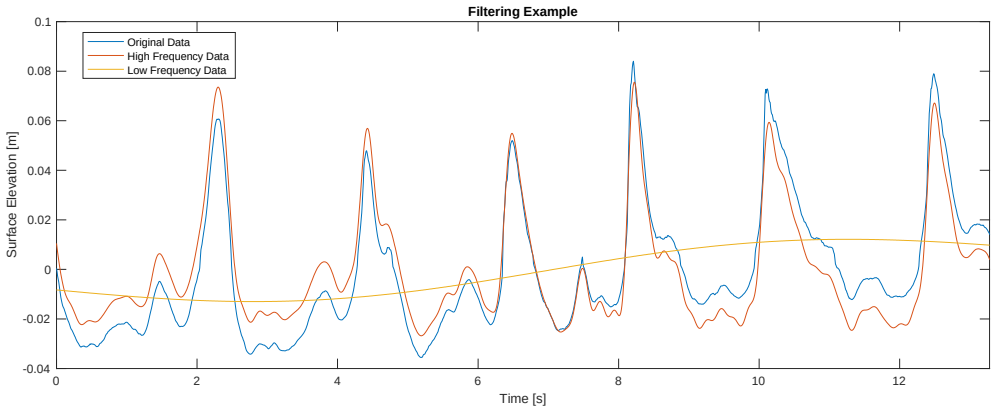

Figure 15: Example of fitlering of high-frequency and low-frequency signals from original free surface elevation

3.2.2 Spatial Tracking of Individual Waves

In order to accurately track individual short waves, the waves needed to be distinguished from one another. The spatial tracking of individual waves was performed by tracking their crests. These can be observed as peaks in the free surface elevation. The computation of the wave tracker worked by iterating over each time step, gathered at 128 Hz, for all 190 gauges. At each time step the free surface elevation was plotted as a function of space. From this, peaks were identified. The identified peaks were labelled in ascending order, starting at the most offshore location (nearest to the wavemaker). The first new peak to enter the system was labelled number 1, the second number 2 etc., as visualised in Figure 15. Through trial and error, it turned out that the crests were only identified when higher than 0.005 m and when they are spaced at least 6 gauges apart. For this reason, the local bumps that arise within the surf zone because of non-linear interactions, were less likely to be identified as actual waves (e.g. see Figure 15 at x > 40 m).

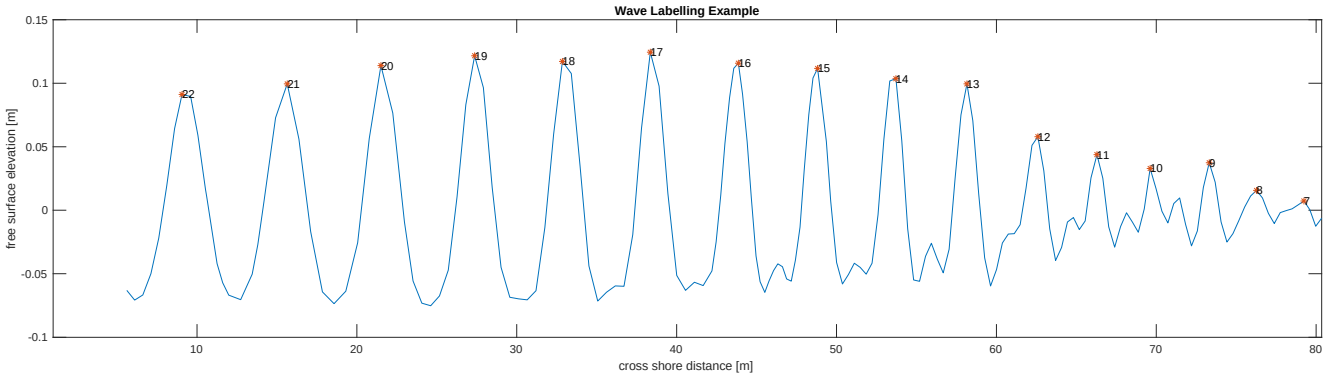

Figure 16: Example of wave labbeling and tracking algorithm

For each, wave the non-linearity parameters (as described in section 2.2) needed to be determined. These are expressed as a function of time, not of space. In order to retrieve this information, at each time iteration, for each identified peak, a time window was specified.

Within this time window, the current crest and preceding crest were identified and the free surface elevation between those points represents the individual wave, see Figure 17. The time window was defined by 100 timesteps (-0.78 sec) forwards and 500 backwards (3.9 sec). This was done, seeing that, with a spatial resolution of 190 gauges, the free surface elevation of the crest, as determined by the spatial tracking, might not correspond with the actual crest of the wave. In other words, the actual crest of the wave could be located in between to gauges. By defining a time window that spanned longer than the total period of the wave, it was guaranteed that the actual crest is found. In this time window again two peaks were identified, and the wave is *snipped* between those and later used for calculation.

Despite the data being detrended, it turned out that it is easier to separate waves by their crests, rather than by the positive to negative zero crossing, which is the more formal way of identifying individual waves. The previously mentioned bumps, that develop in the shoaling zone, could result in multiple positive to negative zero crossings within a single wave. This can be seen in Figure 17, at $x \approx 1.6\,s$. Further shoreward these bumps became more pronounced, complicating the identification of which exact zero crossing is of the original individual wave. This informs the decision to snip waves at the tracked and preceding crest.

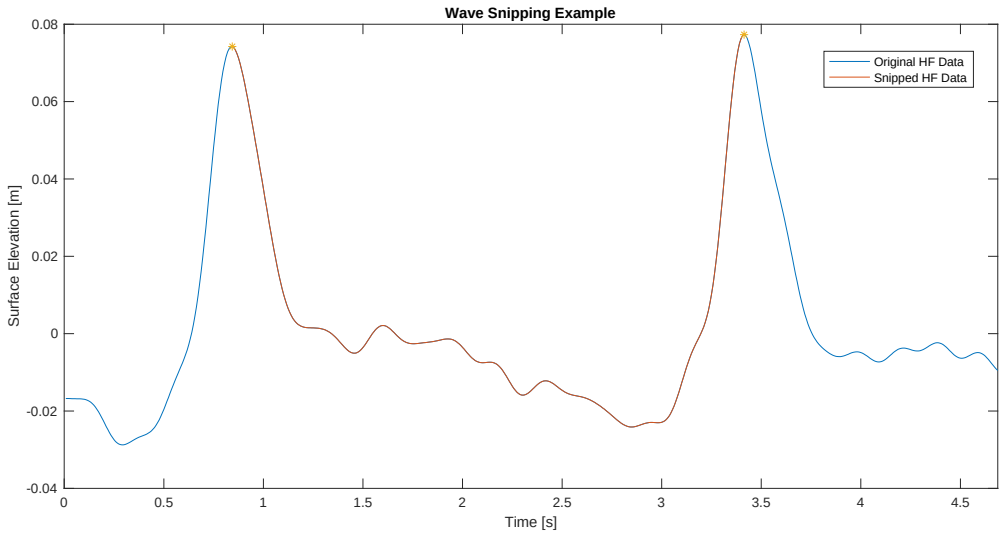

Figure 17: Example of "snipping" individual wave from time series

Close to the offshore boundary, where waves behaved fairly linearly, identification of individual wave crests was straightforward. Within the surf zone, this became increasingly complex. Despite identifying waves at their crest and setting a minimal surface elevation value in combination with a minimal number of gauges that individual waves should be apart, the tracking algorithm sometimes failed to correctly identify the actual movement of the remainder of a wave within the surf zone. For example, it was possible that a local bump generates a higher surface elevation than the remainder of an individual short wave, that has already broken. In this case the algorithm would identify that bump as the new location of the tracked wave. In such a situation, the location of the incorrectly tracked wave suddenly moves seaward. This was identified as un-realistic behaviour and the tracking process was

stopped. Also, a jump forward in space, signified by the location of a tracked wave skipping a gauge, is another criterium to stop the process of wave tracking.

With these mechanisms, the algorithm is capable of accurately tracking a wave to around $x \approx 75\,m$, which corresponds to a depth of ≈ 0.125 m. For the larger short waves, the accurately tracked distance reaches further than this. However, as a significant number of waves would no longer be tracked around $x \approx 75\,m$, the final gauge that was taken into consideration is set at x = 76.3 m.

3.2.4 Individual Wave Parameters

Skewness and Asymmetry

Data retrieved from GLOBEX contained information of the snipped individual wave free surface elevation (η_i) (Fig. 17). The individual wave shape skewness (S_i) was computed as the standard statistical expression of skewness,

$$Sk_i = \frac{<\eta_i^3>}{<\eta_i^2>^{3/2}} \qquad \text{eq. 6}$$

$$As_i = \frac{<H\,(\eta_i)^3>}{<\eta_i^2>^{3/2}} \qquad \text{eq. 7}$$

where the $< \cdots >$ represents averaged over the time series, and the denominator represents the standard deviation of η_i. This was calculated for each individual wave (η_i). The asymmetry (As_i) was computed using the same equation, but by taking its Hilbert transform (Elgar et al., 1987). In this way, waves that are pitching forward will show negative values.

Wave Height, Period and Depth

Wave height was computed by taking the maximum value of each η_i and substracting the minimum η_i (see Equation 5). Wave period was easily be computed as the amount of time steps comprising the snipped wave, multiplied by the recording frequency (128 Hz). Depth (h_i) was computed by taking the mean of the individual snipped wave from the original free surface elevation ($\eta_{i,or}$), meaning it includes set-up and set-down and the infragravity wave induced mean water level offset, and subtracting the depth at the location of the gauge where the wave is identified.

$$H_i = \eta_{i,max} - \eta_{i,min} \qquad \text{eq. 8}$$

Range

In order to assess the variability of both skewness, asymmetry and wave height, the range was computed at each location. This was calculated by determining the maximum and minimum value of both non-linearity parameters per gauge, and then subtracting the minimum values from the maximum. This provides insight in the cross-shore development in wave-to-wave variability.

$$y_{range} = x_{max} - x_{min} \qquad \text{eq. 9}$$

Ursell-number

The Ursell number is a parameterisation of nonlinearity of waves (Doering & Bowen, 1985). Commonly, it is expressed as a function of time averaged wave statistical characteristics. However, in this study it is computed for each individual wave (Ur_i) following Equation 10, and precedingly equation 11 and 12. Where h_i represents depth; a_i represents the amplitude of the wave as a function of the wave height (H_i) and k_i represents the wave number as a function of the wave length (L_i). The latter variable is not computed from the algorithm, and is thus approximated using the wave period (T_i) following linear theory as described by Guo et al. (2002)

$$Ur_i = \frac{3}{4}\frac{a_i\, k_i}{(k_i h_i)^3} \qquad \text{eq. 10}$$

$$a_i = 0.5\, H_i \qquad \text{eq. 11}$$

$$k_i = \frac{2\pi}{L_i} \qquad \text{eq. 12}$$

Infragravity water level variations

The mean water level alterations, as induced by the infragravity waves were also tracked for each individual wave. As stated in 3.2.1 the high frequency and low frequency data have been separated, resulting in data containing information on the short-wave spectrum and the infragravity wave spectrum. For each individual wave, as it travels through the system, the off-set of the mean water level was found by taking the same time frame as the snipped short wave, but from the lower frequency data.

3.2.5 Wave Group Similarity

The GLOBEX wave conditions were defined such that waves are bichromatic. This means that wave groups consist of an integer number of waves and they repeat themselves. In order to assess if waves from different wave groups developped similarly, the cross-shore development of the same wave of different groups is visually compared. The first wave of a

group was determined as the one individual wave crest closest to the crest of the incoming long waves, i.e. the smallest wave of the wave group (Fig. 18b and c). Figure 18a shows that the same individual wave of five different groups develops identical throughout the wave flume for Sk_i, As_i, H_i and Ur_i. For example, there is a distinguishable dip (at $x = 70\,m$) in skewness present for the five waves with label 2, plotted in Figure 18a. This dip is not present for waves with label 5. Ultimately, this means that discussing the development of the individual waves making up a single wave group, will be representative of all waves present in the entire time series. For other experimental settings, see Appendix.

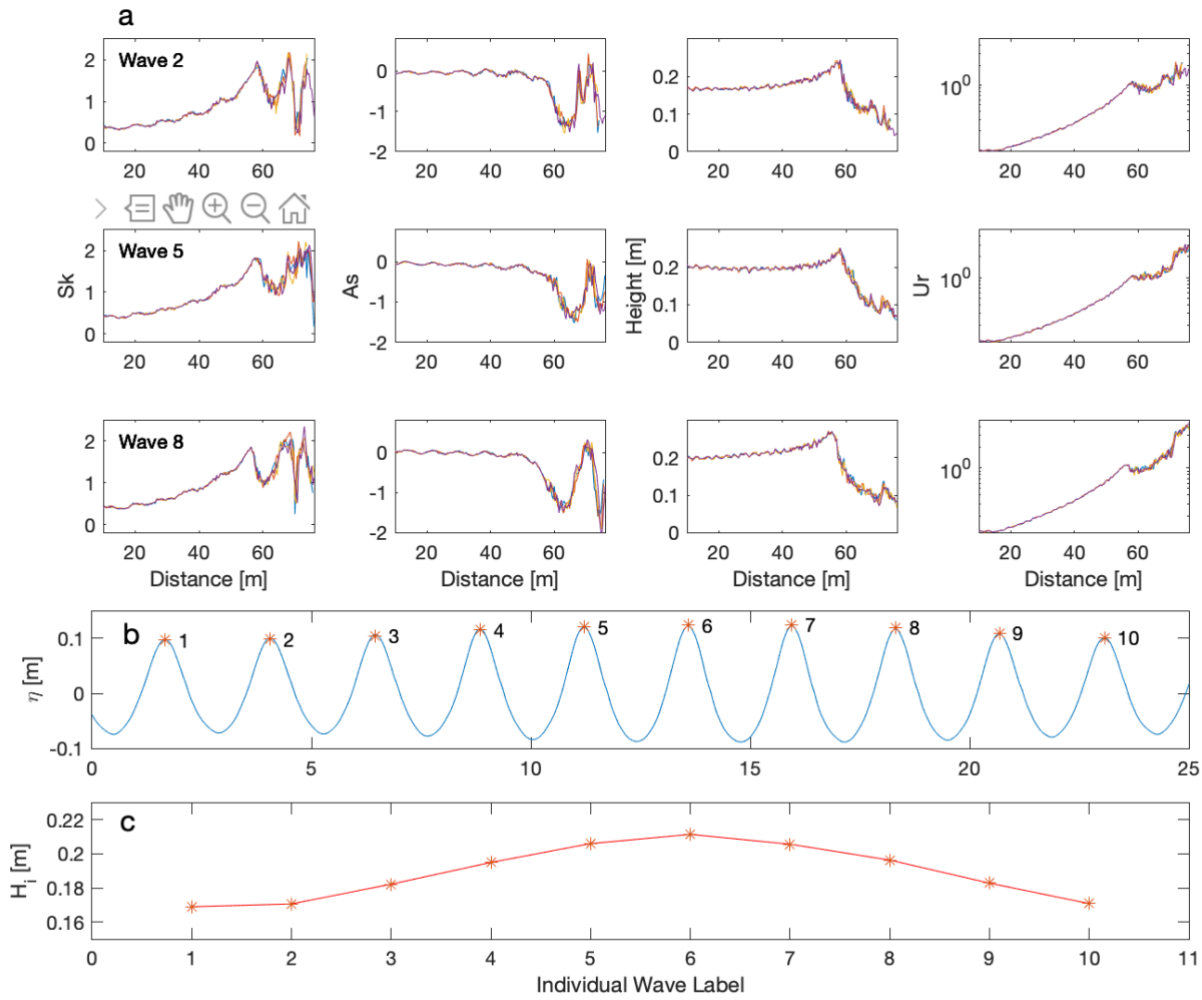

Figure 18: (a) similar development of individual waves from five different wave groups with label 2 (1st row), label 5 (2nd row) and label 8 (3rd row) for Sk (1st column), As (2nd column), H_i (3rd column) and Ur (4th column) as function of distance (m) ; (b) free surface elevation at the first gauge with corresponding wave label; (c) individual wave height at the first gauge plotted as function of wave label.

3.3 SWASH Numerical Model

SWASH is a general-purpose numerical phase resolving model for simulating non-hydrostatic, unsteady, rotational flow, transport phenomena and free surface in coastal waters as driven by tides, wind forces, buoyancy and waves. It is developed by the Technical University of Delft.

It is capable of providing general basis for describing wave transformations from deep water to a beach (TU Delft: SWASH, n.d.). The model was used to simulate an experiment which resembled the GLOBEX experiment as closely as possible, over a similar slope (1:80), in order to validate the use of the model. After the model was ran with similar settings over a steeper sloping beach (1:10).

SWASH was utilised in a one-dimensional cross-shore setting. Similar to GLOBEX it consisted of a wave-maker boundary on the west end and a sloping beach towards the east, positive x-direction. For a full model description, see Zijlema et al. (2011). Within this setting the governing equations can be written as follows:

$$\frac{\partial \eta}{\partial t} + \frac{\partial}{\partial x}\int_{-d}^{\eta} u dz = 0$$

$$\frac{\partial u}{\partial t} + \frac{\partial uu}{\partial x} + \frac{\partial wu}{\partial z} + \frac{\partial wu}{\partial z} = -\frac{1}{\rho}\frac{\partial (p_h + p_{nh})}{\partial x} + \frac{\partial \tau_{xz}}{\partial z} + \frac{\partial \tau_{xx}}{\partial z}$$

$$\frac{\partial w}{\partial t} + \frac{\partial uw}{\partial x} + \frac{\partial ww}{\partial z} = -\frac{1}{\rho}\frac{\partial p_{nh}}{\partial z} + \frac{\partial \tau_{zz}}{\partial z} + \frac{\partial \tau_{zx}}{\partial x}$$

$$\frac{\partial u}{\partial x} + \frac{\partial w}{\partial z} = 0$$

Where *x* is the horizontal coordinate and *z* the vertical. With *z* positive being above the still water level ($\eta = 0$), meaning that $z = -d$ represents the bed level. Where η represents free surface elevation, t represents time, $u(x,z,t)$ and $w(x,z,t)$ are the horizontal and vertical flow velocities, ρ is the density. The hydrostatic pressure is described by $p_h = \rho g(\eta - z)$ and p_{nh} is the non-hydrostatic pressure contribution. Turbulent stresses are represented by τ, and are obtained from a turbulent viscosity approximation. Bottom stress is accounted for by the quadratic friction law at the bottom boundary,

$$\tau_{b,x} = c_f \frac{U|U|}{h}$$

with *h* representing total water depth ($h = \eta + d$), *U* the flow velocity averaged over depth, and c_f the dimensionless friction coefficient determined by the following equation, where *n* represents the Manning friction coefficient and *g* the gravitational constant (9.81 m/s^2):

$$c_f = \frac{n^2 g}{h^{1/3}}$$

3.3.1 SWASH Set-Up

In this study, the model set-up was largely based on earlier work from De Bakker et al. (2015), who previously executed SWASH to resemble the GLOBEX lab experiment. In contrast, to this study they simulated the A-series experiments, which consists of three random short waves conditions. In this research the three bichromatic experiments were reproduced, with wave conditions as described in Table 1.

In order to resolve the wave motion as accurately as possible, a spatial resolution of 0.02 m was chosen; this is sufficient when compared to the wavelength of the dominant wave frequencies. Simulations have been run with a time step of 0.002 s; this corresponds to a Courant number of around 0.3. The bottom boundary layer was defined with a friction coefficient (c_f) calculated with n = 0.015 s/m$^{1/3}$, which is a typical value for unfinished concrete (Chow, 1959).

The wave boundary settings are based on Tissier et al. (2015), who used SWASH to numerically simulate the Van Noorloos experiment (Rijnsdorp et al., 2014). Similarly, to the GLOBEX B-series, these lab data consisted of bichromatic wave conditions. The model was forced with bichromatic Fourier series defined by the parameters: the amplitude for zero frequency in meters (= 0 for all three scenarios), the amplitude in meters (see Table 1), the angular frequencies derived from the wave periods (see Table 1) and the phase (= 0 for all three scenarios). A weakly reflective boundary was utilised in order to avoid rereflection of the long-wave frequencies from the offshore boundary. All three simulations were executed using two vertical layers. Wave breaking was first set to resemble the parametrization as introduced by Smit et al. (2013); α_1 = 0.6 and α_2 = 0.3. However, through trial and error it was found that α_1 = 0.5 correlated better to the GLOBEX derived wave height development.

3.3.2 Free Super Harmonic

When imposing the waves at the offshore boundary, as stated above at a depth of 0.85 meters, significantly present free super harmonics were generated drastically affecting the outcomes of the numerical modelling, especially with regards to non-linearity. This process has been described by Hughes (1993), who found that in all laboratory generated wave experiments, first order wave-maker theory is violated, resulting in the presence of unwanted free super harmonics. These forced waves then create unwanted non-linearities (see Fig. 19). Especially within this research, which focuses on non-linearities, these free super harmonics are highly unfavorable. Both Hughes (1993) and Schäffer (1994) suggest second-order wave maker theory to generate actual regular waves. It is for this reason, the piston type wave maker was steered with signals in Series A and B, that were calculated with second-order wave generation (Ruessink et al., 2013).

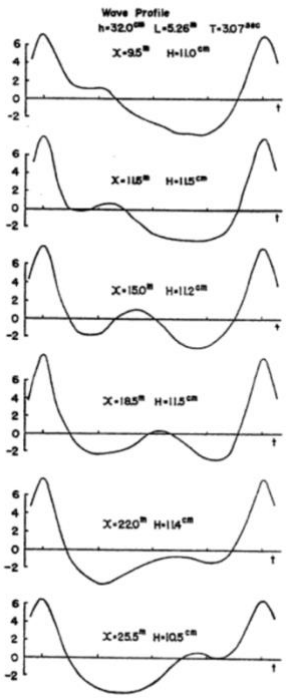

Figure 19: Motion of free super harmonic (Hughes, 1993)

In order to account for this, second-order wave maker theory could have been applied in SWASH, but this is of very complex nature, if at all possible. In addition, when depth is increased, this phenomenon is much less present. For that reason, it was decided to increase the numerically modelled domain compared to GLOBEX. Instead of starting at a depth of 0.85 m, the domain is lengthened at the off-shore boundary starting at depth of 1.85 m, then following a similar bed slope to the GLOBEX bed slope of 1:80, until a depth of 0.85 m is reached. From there, the bottom closely follows GLOBEX closely (Fig. 20). The bottom contour was defined with the same spatial resolution of 0.02 m, with a slope of 1:80 m after a flat section. The total length of the simulated area was 200 meters, of which the latter 100 meters were investigated in this study.

Figure 20: Bottom contour as used for SWASH validation

3.3.3 Model output

The model generated two different forms of output. Both forms contain free surface elevation (η) of the water, similar to GLOBEX at 128 Hz. One file contains the free surface elevation of 1000 points (gauges) spread evenly along the cross-shore profile of the complete simulated area. Thus, including the first half of the bottom contour starting at a depth of 1.85 m. As the total simulated area consists of 200 meters, this means that dx = 0.2 m. This results in a total of 500 gauges in the area of interest, which is considerably more than the 190 of GLOBEX. Another output file was created containing η at the exact locations of the GLOBEX gauges, also at 128 Hz. The latter data file equals the GLOBEX output form.

3.3.4 SWASH validation

Figure 21 shows the development of significant wave height (a), skewness (b) and asymmetry (c) for both the modelled and measured data from series B2. These four variables are compared using linear regression validation and the related R^2-values are presented all three experimental settings (B1, B2 and B3) in Table 3. It is important to note that, for validation, these bulk variables are computed for the entire laboratory and modelled time series, and do not represent the development individual waves. The development of significant wave height has been prioritised. The overall cross-shore development of significant wave height and

breaking is captured well for all three cases, signified by high squared correlation values ($R^2 \approx 0.98$).

With regards to skewness and asymmetry, from Figure 21b and c it becomes apparent that the development of non-linearity is captured well up to $x \approx 60\ m$. From here to $x = 70\ m$ the general trend of a decrease followed by an increase in skewness and asymmetry is captured. However, the modelled skewness results in an under estimation at $x \approx 65\ m$. At this same location an under estimation (less negative) values for asymmetry is found. From here shoreward the non-linearity is not captured well. This is represented by squared correlation values that are lower ($R^2_{Sk} \approx 0.78$ and $R^2_{As} \approx 0.74$).

Figure 21d shows the variance density spectra of GLOBEX and SWASH captured at $x = 10\ m$. For this, it is apparent that the modelled boundary wave conditions indeed align with those of the laboratory experiment. This is signified by the squared correlation values for all three experimental setting ($R^2_{Var.Den.} = 0.99$). Despite this, it should be noted that in the modelled experiment more noise is present. This is represented by the higher values in between the primary wave frequencies and their sub- and super harmonics.

The development of wave height was prioritised to be the main validation variable, the corresponding squared correlation coefficient values are sufficient. Notably, the non-linearity is captured reasonably well, especially in the offshore area. Under estimations occur between $x \approx 60\ m$ and $x \approx 70\ m$. From here shoreward, the development of skewness and asymmetry shows no correspondence. However, SWASH will be utilised to stimulate waves over a steep sloping bed (1:10). Rocha et al. (2017) showed that, on a steep bed slope, skewness and asymmetry are less pronounced. For this reason, it is believed that these model settings are correctly validated and will suffice for the purpose of this study.

Table 2: R^2-values for validation of modelling approach for B-Series

Series	***B1***	***B2***	***B3***
Significant Wave Height	0.97	0.98	0.98
Skewness	0.84	0.74	0.77
Asymmetry	0.83	0.61	0.79
Variance Density	0.99	0.99	0.99

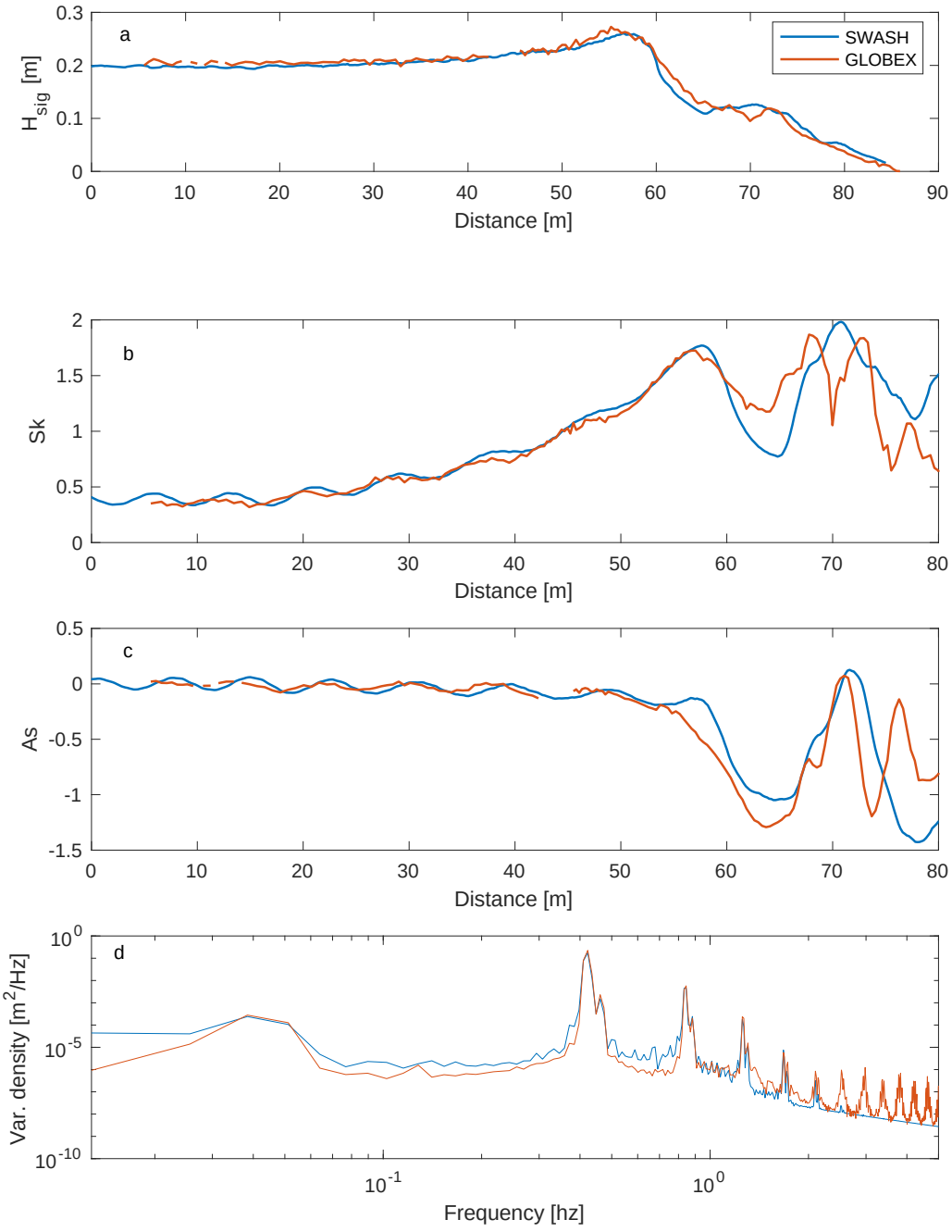

Figure 21: Comparison of experimental setting B2 between laboratory and modelled (a) significant wave height, (b) skewness, (c) asymmetry and (d) variance density

3.2.5 Set Up Steep simulation

The bottom profile for the steep (1:10) simulations is shown in Figure 22. Similar to the validation set up, the profile starts with an approach on a gentle slope (1:80) in order to minimize the effects of the discussed free super harmonics. After the flat section a steep bed slope (1:10) is implemented. The complete simulated domain is reduced from 200 meters to roughly 130 meters. Despite the area of interest being reduced a fair bit, the Courant number is not altered too much. This study focusses on the area of $x > 100\,m$. The boundary wave conditions of B1, B2 and B3 (Table 1) have been simulated over this steep bed profile and the corresponding experimental settings are called S1, S2 and S3. Figure 23 shows the space-time diagrams of the free surface elevation (η) of both the physical experiment GLOBEX over a 1:80 bed slope and the modelled experiment in SWASH over a 1:10 bed slope.

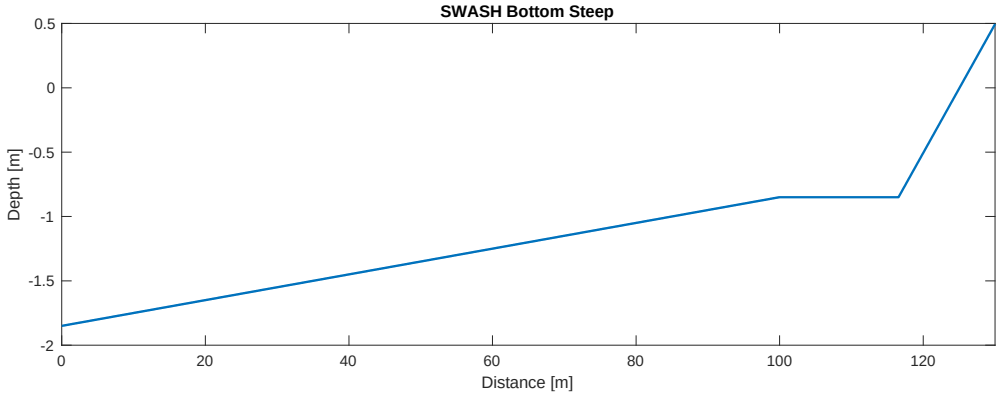

Figure 22: Bottom contour for steep simulation, S-series

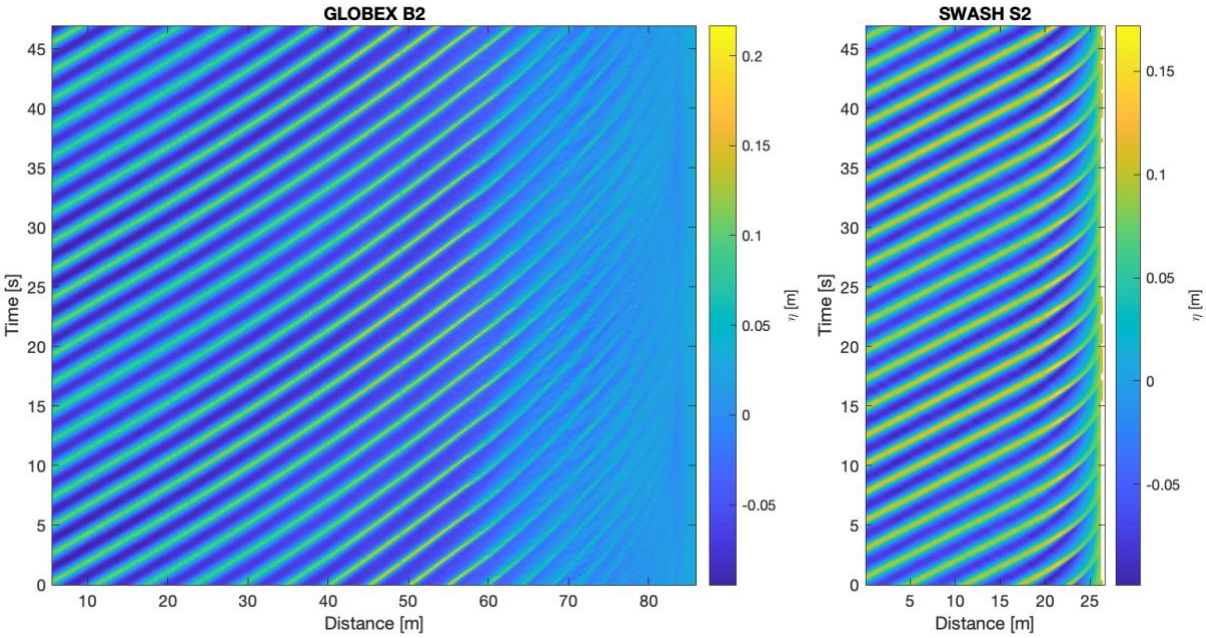

Figure 23: Space time diagram of free surface elevation for B2 and S2

4. Results

Figures 24 to 26 (B-series) and 28 to 30 (S-series) visualise the development of skewness (A), asymmetry (B), infragravity induced water level off-set (C), wave height (D) and Ursell number (E) for all individual waves making up one wave group from each of the six experimental settings. In addition, the location of the wave breaking zone is computed and visualised with vertical dashed lines in the wave height plots (D) from the development of wave height. The area seaward of the offshore dashed line is considered the shoaling zone. This line signifies the location where the largest wave of the group starts breaking. The second dashed line signifies the most shoreward location where an individual wave starts breaking. The area between these dashed lines is regarded as the outer breaking zone. Landward of the second dashed line, all waves are breaking. This is considered the inner surf zone. Figures 27 (B-series) and 31 (S-series) show the cross-shore development of the range in skewness, asymmetry and wave height. The wave conditions for each experiment are as specified in the previously presented Table 1. Firstly, general observations for all three B-series experimental settings are presented, followed by a detailed quantitative analysis of results of setting B1. Finally, the differences andsimilarities for all three GLOBEX B series are discussed. After, this same structure is applied to the results of the SWASH S series.

4.1 Individual Wave Development of GLOBEX

4.1.1 Series B in general

The cross-shore development of individual waves for B1, B2 and B3 is presented in Figure 24 – 26, Figure 27 shows the development of range. Due to the bichromatic nature of the wave conditions at the offshore boundary a clear variability of wave heights is present, with $H_{i,range} \approx 0.04\,m$ for B1 and B2, and $H_{i,range} \approx 0.12\,m$ for B3. As a consequence of shoaling, individual wave heights start to increase slightly from $x \approx 30\,m$, $z = 0.675\,m$ onwards. This increase continues towards the breaking point, which, for the larger waves of the group, is located at $x \approx 55\,m$, $z \approx 0.358\,m$. With regards to the infragravity wave induced mean water level offset, all three experimental settings show clear patterns of a standing wave, with nodes and antinodes. The infragravity waves display a progressive pattern shoreward, signified by less-defined nodes and antinodes and a larger range at the landward boundary. This is consistent with the imperfect shoreline reflection of the infragravity wave, as noted by Ruessink et al. (2013) and De Bakker et al. (2015).

In all three cases $Sk_i \approx 0.25$ and $As_i \approx 0$ at the offshore boundary. Shoreward these remain constant with relatively small wave-to-wave variability ($Sk_{i,range} \approx 0.15$) when compared to wave height. It should be noted that, despite efforts to cancel the presence of the free super harmonic, it seems as though it is still present (minor rises and depressions for Sk_i and As_i in the shoreward direction for all waves of each experimental setting). When

depths reduce in the shoaling zone, an increase in skewness initiated at $x \approx 25\,m$, $z = 0.740\,m$ is observed, while asymmetry remains constant at $As \approx 0$. The wave-to-wave variability increases just landward of the breaking zone (at $x > 50\,m$), especially in B3 with $Sk_{i,range} \approx 0.70$. Local maxima for skewness are reached here with $Sk_i > 1$ and $Sk_{i,max} \approx 2$.

At the offshore boundary and throughout the shoaling zone the range of asymmetry remains fairly constant with $As_{i,range} \approx 0.10$ for B1 and B2 and $As_{i,range} \approx 0.40$ for B3. Just before and in the outer breaking zone, $x > 55\,m$, $z = 0.430$, individual waves start to pitch forward and eventually break, forcing As_i to become negative and display an increase in wave-to-wave variability. Here all individual waves from the three cases become increasingly negative, and $As < -1$ within the breaking zone. At this location values for skewness reduce. This is expected behaviour of both non-linearity parameters as described in Section 2.2.1. However, in the inner surf zone, shoreward from $x > 64\,m$ the skewness increases again, and the asymmetry reduces. At $x = 70\,m$, $z = 0.174\,m$ behaviour shows strong wave-to-wave variability, best seen for case B2 (Figure 25a and b), with Sk_i values becoming negative for some waves and for others remaining ≈ 1.5, with corresponding range values for all three cases of $Sk_{i,range} \approx 1.60$. At this location asymmetry reduces (becomes less negative). Here wave height (H_i) increases slightly, indicating a reduction in wave breaking.

In all three B-series cases $Ur_i \approx 0.1$ at the offshore boundary. In the shoaling zone, this increases exponentially towards the breaking point, where $Ur_i \approx 1$. Here Ur_i remains fairly constant for most waves. From $x > 65\,m$ the Ur_i increases again, with an increase in wave-to-wave variability. Most waves remain between $Ur_i = 1\ and\ 2$, some waves reach their maximum value at the shoreward end with $Ur_{i,max} \approx 3$.

4.1.2 Series B1 in detail

Figure 24 presents the development of characteristics of the six individual waves (labelled 1-6), making up one wave group, from experimental setting B1. The individual wave height (H_i) at the offshore boundary ranges from 0.173 m to 0.214 m, with $H_{i,range} = 0.04\,m$. This indicates a difference of 19% in wave height. Up until $x = 30\,m$ the wave-to-wave variability seems to remain fairly constant for most waves. However, this does not apply to individual waves, e.g. wave label 1 is the smallest at the offshore boundary with H_i = 0.173 m, at $x = 30\,m$ this has increased to 0.190 m. At the breaking point of this individual wave $H_i = 0.279\,m$, the second largest individual wave height out of these 6 waves. It is for this reason that this wave is the one of two to break furthest offshore.

Notably, it is this same wave that shows a decrease in the infragravity mean water level offset ($\eta_{i,ig}$) (Fig. 24C). At the offshore boundary this is $\eta_{i,ig} = 1.591 * 10^{-3}\,m$. At the break point of the individual wave, the infragravity offset reaches the minimum value of the wave group of $\eta_{i,ig} = -6.845 * 10^{-3}\,m$. This indicates that the development of infragravity induced water level offset negatively correlates to the individual short wave height. This short

wave developed from smallest to largest wave of the group, as it reached the breaking zone and consequently breaking is initiated furthest offshore. The initial largest short wave of the group (label 4) with $H_i = 0.214\,m$, shows the least growth through the shoaling zone when compared to the other waves and breaks furthest shoreward with $H_i = 0.255\,m$ at $x = 58.5\,m$. The infragravity wave induced mean water level offset for this wave shows an increase from $\eta_{i,ig} = -1.735\,e^{-3}\,m$ at the offshore boundary and $\eta_i = 6.648\,e^{-3}\,m$ within the break point. This indicates a relation between infragravity wave induced mean water level off set and the individual wave height. However, when looking at wave label 2 and 6, which have similar infragravity induced mean water level offset in the breaking zone, these waves have a different wave height within the breaking zone and break at different points. Wave label 2 breaks at $x = 54.45\,m$, with a maximum height of $H_i = 0.273\,m$, whilst wave label 6 breaks further shoreward at $x = 55.56\,m$, with a maximum height of $H_i = 0.263\,m$.

The development of skewness is similar for all six waves in the offshore area. At the offshore boundary $Sk_i \approx 0.4$ (with $Sk_{i,range} = 0.06$) and increases for all waves to $Sk_i \approx 0.9$ at $x = 40\,m$, with increased range $Sk_{i,range} = 0.12$. Slight depressions and rises are observed, which may be caused by presence of a free superharmonic signal. In the offshore area minor wave-to-wave variability is present for Sk_i, in the order of 0.01 to 0.10. From $x = 40\,m$ towards the breaking zone at $x = 54.8\,m$ the wave-to-wave variability in skewness increases to $Sk_{i,range} \approx 0.30$, where for wave label 6 $Sk_i = 1.86$, and for wave label 3 $Sk_i = 1.56$. At the point of breaking, the shortwave height of wave label 1 just exceeds that of wave label 6 (with 0.01 m). However, towards the end of the shoaling zone, wave label 6 was the largest wave. This turns out to have a stronger effect on the skewness as wave label 6 reaches a larger value for maximum individual skewness within the breaking zone with $Sk_i = 1.91$, while wave label 1 reaches a maximum value of $Sk_i = 1.84$. Interestingly, the smallest short wave (label 4), which is the wave to break closest to shore at $x = 58.5\,m$, ultimately reaches the highest value for skewness with $Sk_i = 1.98$ at this same location. Also, this wave has shown the highest (most positive) values for the infragravity induced mean water level offset within the breaking zone. The maximum range in individual wave height in the outer breaking zone $= 0.57$. From here shoreward, the skewness of all waves reduces to approximately $Sk_i \approx 1$.

From $x > 63\,m$ shoreward, the skewness increases again for all six waves, but with a wider range than further offshore ($Sk_{i,range} = 1.68$), while individual wave heights keep decreasing as a consequence of breaking. At $x = 70\,m$, there is a remarkable dip in skewness, for waves label 2 and 3. This is not the case for the other waves. At this same location an antinode can be observed for $\eta_{i,ig}$. After this point, the skewness of the waves that indicated this dip rises again to $x \approx 73.3\,m$ where range reduces ($Sk_{i,range} = 0.69$), after which the values for Sk_i reduce towards the end of the wave tracking capabilities of the applied methods.

The development of asymmetry is similar for all six waves in the shoaling zone, where at the offshore boundary $As_i \approx 0$, until $x \approx 50\,m$. When compared to the skewness in this area the asymmetry of individual waves shows more wave-to-wave variability, with

$As_{i,range} \approx 0.15$, and fairly constant this throughout the shoaling zone. When approaching the breaking zone, the asymmetry increases, which is indicated by values becoming more negative. Notably, the larger two waves in the breaking zone (wave label 1 and 6) show a stronger reduction further offshore As_i, indicating these waves then become more asymmetric. Wave label 3 and 4 develop in correspondence with their wave height and, with their breaking point being closest to shore, initiate a decrease in As_i more landward, at $x = 58.5\ m$. In the breaking zone we find $As_{i,range} \approx 0.57$. From here all six waves continue to become more asymmetric, showing values of $As_i \approx -1.2$. In addition, at the $x \approx 64\ m$-mark, the wave-to-wave variability is reduced. After this point, the asymmetry reduces (to $As_i \approx 0$) at a different rate for the individual waves, with the wave-to-wave variability increasing again to a maximum of $As_{i,range} \approx 1.86$. Wave label 2 and 3 peak just after $x \approx 70\ m$, even reaching positive values. Interestingly, this coincides with the waves that drastic dip in the development of Sk_i, after which they become strongly asymmetric again, reaching maximum values of $As_i \approx -1.7$. Waves label 4 and 5 show different behaviour and slowly approach $As_i = 0$, which these waves reach at the most shoreward location.

4.1.3 Series B: differences and similarities

In experimental setting B3, group modulations were enhanced by decreasing amplitude a_1 and increasing a_2 (Table 1). This is confirmed by the individual development of wave height, showing a much greater wave-to-wave variability at the offshore boundary (Fig 25D, 26D and 27D), with a range of $H_{i,range} \approx 0.04\ m$ for B1 and B2 and $H_{i,range} \approx 0.12\ m$ for B3. As a result of shoaling, this variability is amplified towards the breaking zone, causing the breaking zone to be much wider when compared to B1 and B2, as larger waves break further offshore when compared to the smaller waves. B1 and B2 have an outer breaking zone width of 4.4 m and 4.1 m, much smaller compared to the 10.7 m wide outer breaking zone of B3. Within these zones the maximum ranges with regards to wave height are found with $H_{i,range} \approx 0.09\ m$ (B1), $0.12\ m$ (B2) and $0.17\ m$ (B3), seaward a gradual decrease is observed for all three experimental settings.

With regards to the infragravity wave induced mean water level offset, nodes and antinodes are located at e.g. $x \approx 25\ m$ and $x \approx 50\ m$ for B2 and B3, which contain a similar f_3 frequency (0.441 Hz) and thus corresponding wavelength. For B1, which has a different f_3 (0.433 Hz) the nodal shape is shorter with nodes located at e.g. $x \approx 15\ m$ and $x \approx 35\ m$. The infragravity waves display a progressive pattern shoreward, indicated by less-defined nodes and antinodes and a larger range. Just after the breaking point $x > 59\ m$, the infragravity wave induced mean water level offset shows deviations from the general trend, with pronounced spikes that approach $\eta_{ig} \approx 0$. This is less pronounced for B3. The enhanced group modulation of B3 is evident from η_{ig}. Around the breaking point this water level offset ranges from $\eta_{ig} = 1.94e-2\ m\ to -1.95e-2\ m$, which is about twice as pronounced, when compared to B1 and B2.

Throughout the shoaling zone, the development of skewness creates a much wider range for case B3, this continues throughout the surf zone. For this experimental setting, the range increases from $Sk_{i,range} = 0.13$ (for all three settings) at the offshore boundary, to $Sk_{i,range} = 0.75$ at the end of the shoaling zone. Simultaniously, for B1 and B2 an increase in wave-to-wave variability is observed to $Sk_{i,range} = 0.3$, in the outer breaking zone. With regards to asymmetry, the offshore variability is much stronger for B3, when compared to B1 and B2, which only show minor variability offshore from the breaking point. The values for asymmetry at the offshore boundary range from $As_i = -0.16$ to $As_i = 0.16$ for B3 with $As_{i,range} = 0.32$, for B1 and B2 $As_{i,range} \approx 0.10$ is observed. This variability remains constant throughout the shoaling zone and increases just before and within the outer breaking zone, where maximum values of $As_{i,range} \approx 0.57$ (B1), 0.93 (B2) and 1.52 (B3) are found. After, a reduction around $x \approx 65\ m$ and an increase in wave-to-wave variability is observed in the inner surf zone for all three cases. Maximum values of $As_{i,range} \approx 1.8$ are found for all three cases. Finally, in the case of B3, the variability in Ursell is wider along the whole profile, reaching maximum values when the largest waves start to break. This can be directly appointed to the larger variability in wave height along the full profile.

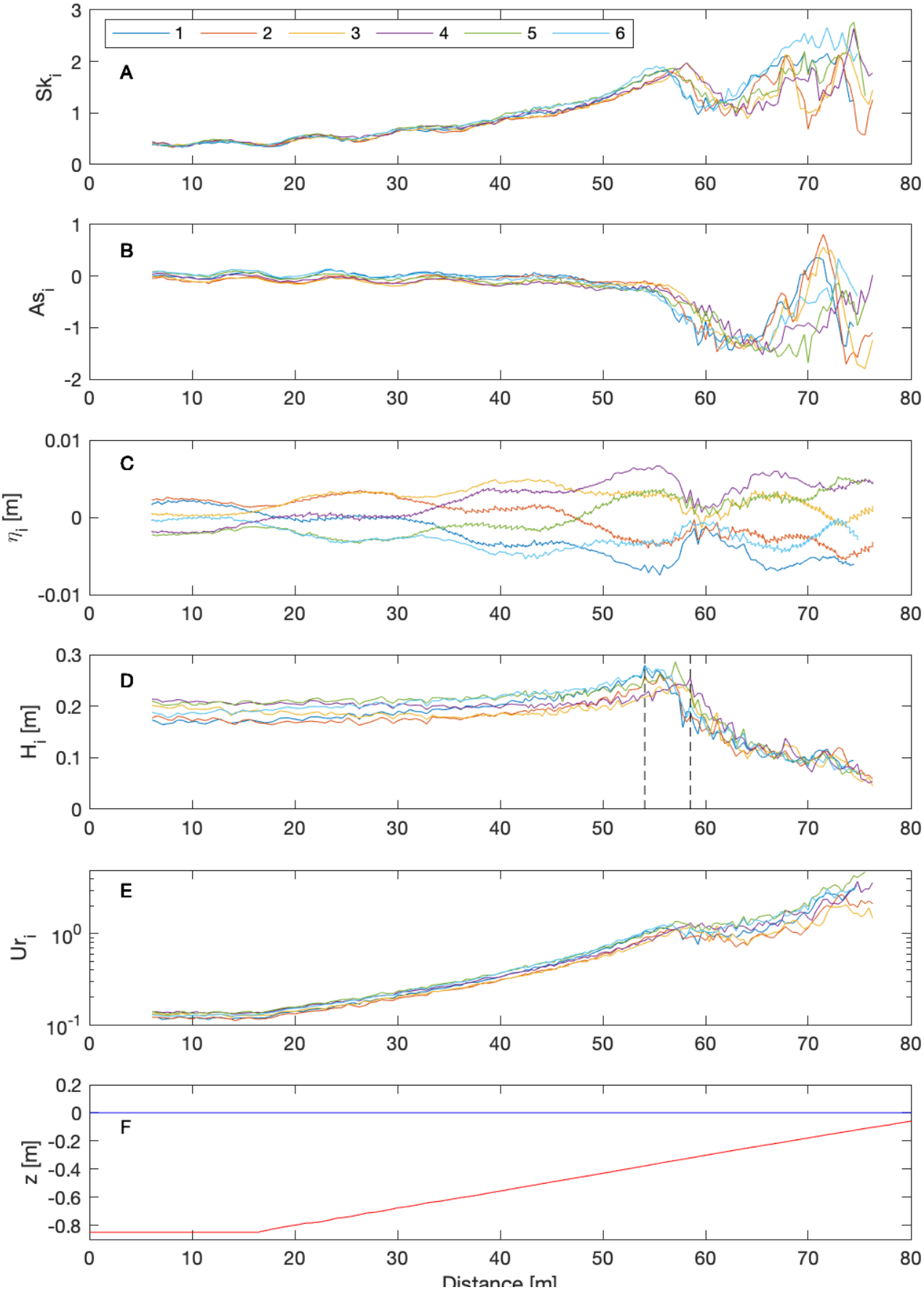

Figure 24: cross shore development for B1 of individual wave (a) skewness, (b) asymmetry, (c) infragravity wave induced mean water level offset, (d) height, (e) Ursell-number and (f) bottom contour (red) and still water level (blue)

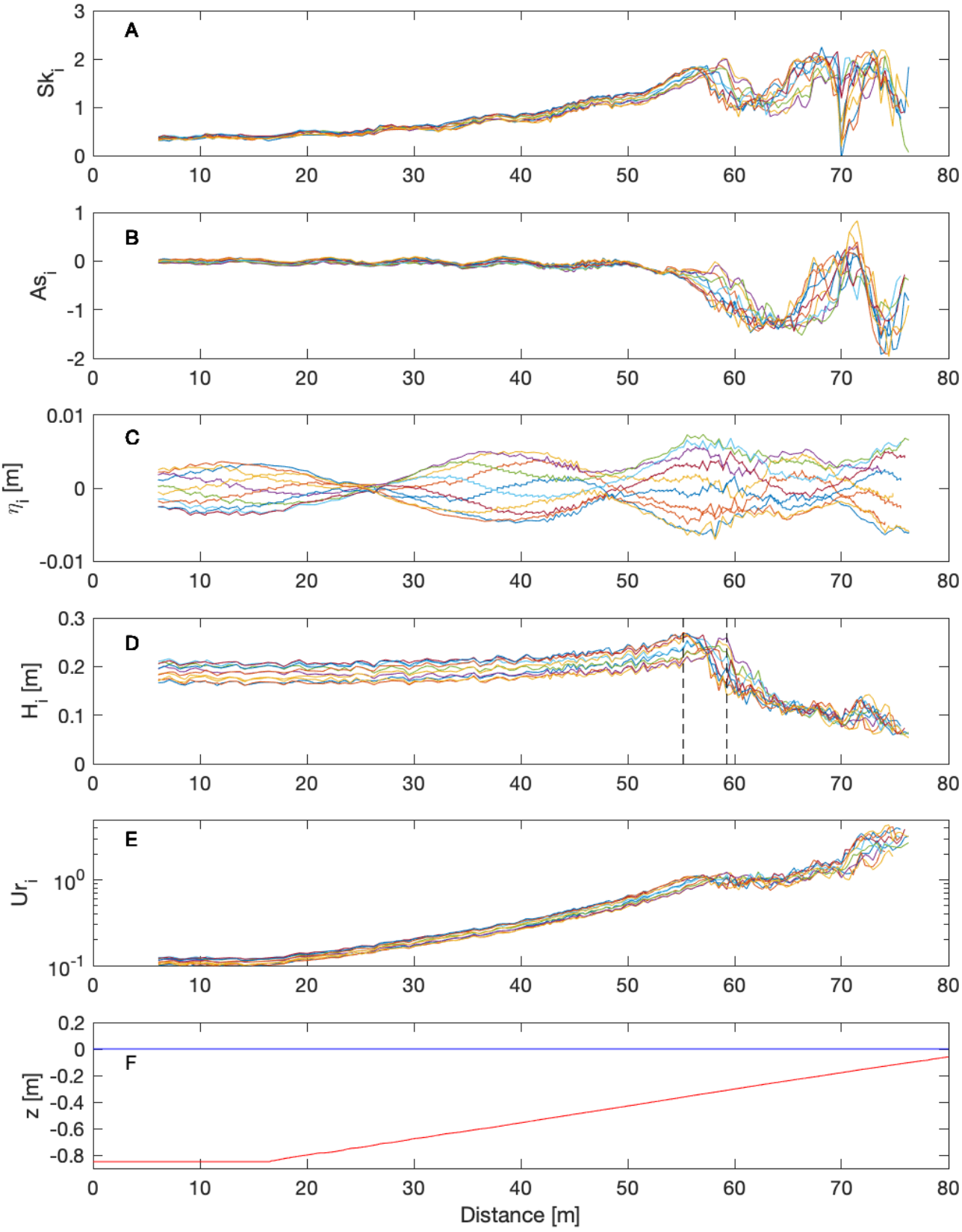

Figure 25: cross shore development for B2 of individual wave (a) skewness, (b) asymmetry, (c) infragravity wave induced mean water level offset, (d) height, (e) Ursell-number and (f) bottom contour (red) and still water level (blue)

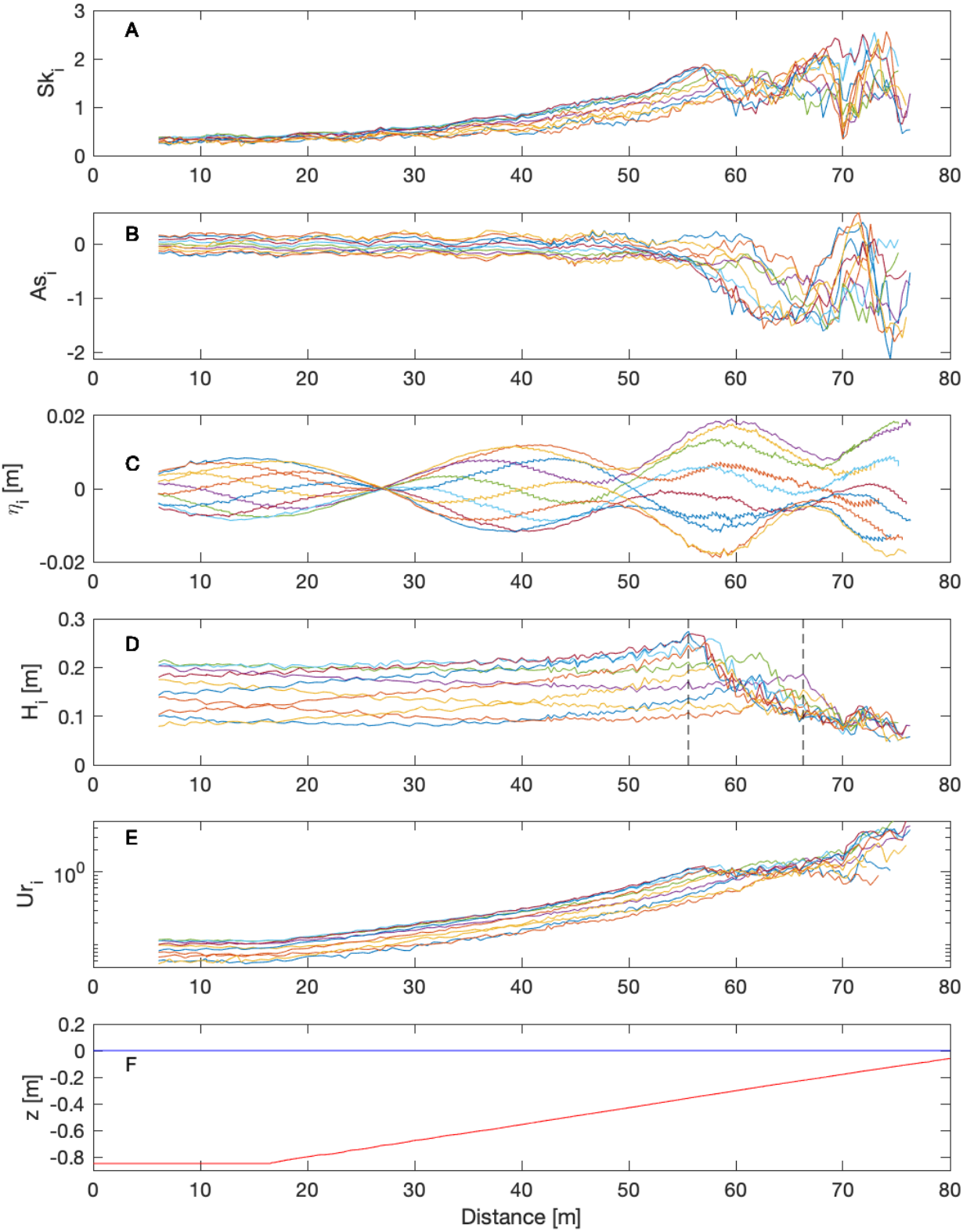

Figure 26: cross shore development for B3 of individual wave (a) skewness, (b) asymmetry, (c) infragravity wave induced mean water level offset, (d) height, (e) Ursell-number and (f) bottom contour (red) and still water level (blue)

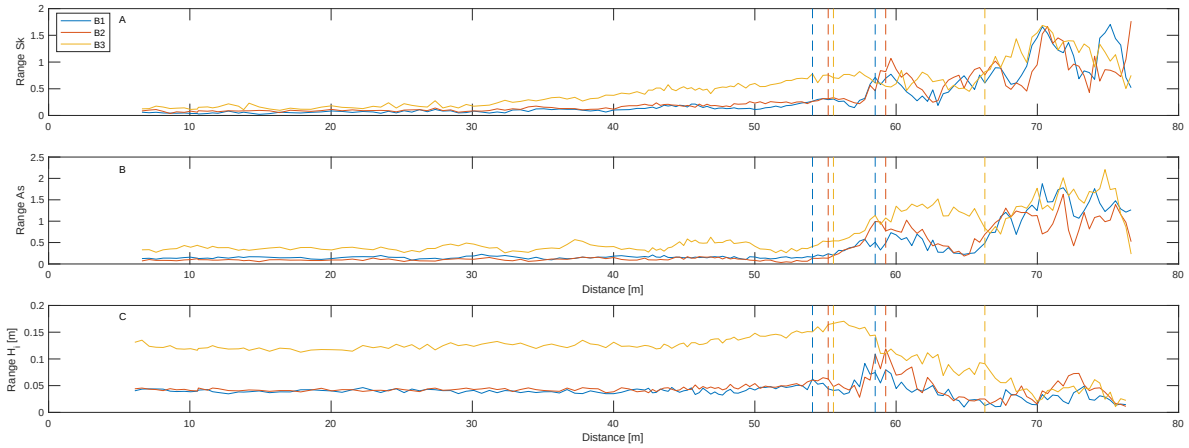

Figure 27: Development of range in individual (A) skewness, (B) asymmetry and (C) wave height (m), expressed as function of distance (m), for B1 (Blue line), for B2 (Red line) and B3 (Yellow line)

4.2 Individual Wave Development of SWASH

4.2.1 Series S in general

In series S, through modelling, bichromatic waves propagated over a steep sloping bed (1:10). At the offshore boundary a clear variability of wave heights is present, showing similar values to the wave conditions of the B series, with a range of $H_{i,range} \approx 0.04\ m$ for S1 and S2 and $H_{i,range} \approx 0.12\ m$. The short wave height remains constant up until $x = 17\ m$, from here the steep bottom contour reduces the depth shoreward. From the location of initiation of the bed slope shoreward ($x > 17\ m$), the effects of shoaling are observed as wave heights increase towards their breaking point ($x = 21\ m$), from $H_i \approx 0.18$ to $H_i \approx 2.3$. The range slightly increases to $H_{i,range} \approx 0.05\ m$ for S1 and S2, and with a similar proportion increases to $H_{i,range} \approx 0.15\ m$ for S3. Consequently, S3 displays a much wider breaking zone, with a width of 1.4 m, compared to a width of 0.4 m for both S1 and S2. Notably, the largest individual wave of each the experimental setting breaks at $x = 21.4\ m$. Shoreward of the breaking zone individual wave heights reduce and the variability also reduces.

With regards to the infragravity wave induced mean water level offset, a less defined nodal and antinodal structure can be identified. Possible nodes are found at the following locations: for S1 at $x = 4\ m$ and at $x = 15\ m$, for S2 and S3 at $x = 10\ m$ and $x = 23\ m$. The nodes found in the S-series are observed to be similar to those found closer to the shore for the B-series. As the modelled data incorporates the lengthened bed contour visualised in Figure 22, the progressive behaviour of the infragravity wave is induced outside the investigated area. Within the research area ($x = 0\ m\ to\ 25\ m$) the infragravity waves show no strong progression, with the exception of S3.

In all three cases the skewness and asymmetry demonstrate a 'wobble' in the cross-shore development. This creates some wave-to-wave variability, early at the offshore boundary, with $Sk_{i,range} \approx 0.15$ for all three experimental settings and $As_{i,range} \approx 0.15$ for

S1 and S2, $As_{i,range} \approx 0.35$ for S3. It should be noted that, despite efforts to reduce the presence of the free super harmonic signal, especially with regards to skewness, a minor rise and fall are still present. This is also the case for the B series. Up until the shoaling zone, values are $Sk_i \approx 0.4$ and $As_i \approx 0$.

In the shoaling zone, where wave heights increase slightly, an increase in skewness is present reaching up to $Sk_i \approx 0.9$, at $x = 22$ and $z = 0.326$. After breaking, the skewness reduces to $Sk_i \approx 0.4$. The asymmetry increases just before breaking (at $x = 21.4\,m$), signifying waves becoming steeper. At the shore, asymmetry reaches maximum (negative) values at $As_i \approx 1.8$, at $x = 25$ and $z = 0.006\,m$. Ranges increase slightly in the outer breaking zone with $Sk_{i,range} \approx 0.37$ for S1 and S2, and $Sk_{i,range} \approx 0.65$ for S3. Here, asymmetry ranges are found of $As_{i,range} \approx 0.35$ for S1 and S2, and $As_{i,range} \approx 0.74$ for S3. In the inner surf zone, wave-to-wave variability of both skewness and asymmetry reduces for all experimental settings.

4.2.2 Series S1 in detail

In Figure 28 the development of the investigated characteristics is presented for each individual wave in the cross-shore direction for S1. The wave groups in this series consist of 6 waves. The individual wave height at the offshore boundary ranges from $H_i = 0.169\,m$ to $H_i = 0.211\,m$, which indicates a 16% difference in H_i near the wavemaker and a range of $H_{i,range} \approx 0.15\,m$. Throughout most of the investigated area, this remains fairly constant, showing minor deviations. At $x = 17\,m$, where the incline in bed slope is initiated, up until the breaking zone which starts at $x = 21.4\,m$, the effects of shoaling are observed with increasing individual wave heights (to $H_i \approx 0.235\,m$). The individual waves develop differently with regards to their height; at the offshore boundary wave label 1 and 2 show similar heights $H_i \approx 0.20\,m$. At the outer breaking zone wave label 2 has remained the largest wave of the group and has undergone an increase in height to $H_{i,max} = 0.268\,m$ at $x = 21.4\,m$, whilst wave label 1 reaches $H_{i,max} = 0.254\,m$ at $x = 21.8\,m$.

With regards to the development of skewness of individual waves in series S1,a general trend with rises and depressions (at $x = 7\,m$ and $x = 15\,m$) can be perceived. This is the result of the present free super harmonic. Values of skewness fluctuate between $Sk_i = 0.55\ and\ 0.25$, up until $x = 17\,m$. Around these, some wave-to-wave variability is observed and appointed to short wave reflection on the steep beach slope. In the shoaling zone ($x = 17\,m\ to\ 21\,m$), skewness increases to $Sk_i \approx 0.90$. Wave label 2 and 3 are found to have the largest individual wave height in the breaking zone and correspondingly show maximum values with $Sk_i = 0.965$ for wave label 3 and $Sk_i = 0.958$ for wave label 3. Just after the outer breaking zone, some trend breaking behaviour is observed, with spikes in individual skewness (both positive and negative). Correspondingly, at this location the largest range of skewness is observed with $Sk_{i,range} \approx 0.41$.

The development of the asymmetry is more uniform. Also, here the effects of the free surface elevation are observed (with slight rises and depressions). Up until $x = 17\,m$, we

find $As_i \approx 0$, with a range of $As_{i,range} \approx 0.02$. Towards the breaking point, where asymmetry becomes more negative, no increase in range is observed. All waves develop similarly and reduce to a negative maximum of $As_i \approx 1.8$ at the shore. Ursell shows similar uniform development, with minor deviations caused by the slight differences in wave height, but apart from that no variability is observed.

4.2.3 Series S: differences and similarities

Similar to the B series, in experimental setting S3, group modulations were enhanced. This is clearly demonstrated by the individual wave height at the offshore boundary showing a stronger variability when compared to those of S1 and S2. This translates into a range of $H_{i,range} \approx 0.04\ m$ for S1 and S2, and $H_{i,range} \approx 0.12\ m$ for S3. The larger difference in wave heights results is a wider breaking zone. In the case of S1 and S2, starting at x = 21.4, the breaking zone expands 0.4 m wide. For S3, also starting at x = 21.4, the outer breaking zone has a width of 1.8 m. Within the outer breaking zone, the largest range in wave height is observed with a proportional increase of $\approx 20\ \%$ compared to the offshore range for all three cases. These enhanced group modulations are also apparent in the infragravity induced offset, resulting in larger positive and negative values. At maximum the variability offset is 1 order of magnitude larger when compared to S1 and S2, ranging from $\eta_{ig} = 0.01\ m$ to $\eta_{ig} = -0.01\ m$.

With regards to nonlinearity, a similar variability in skewness ($Sk_{i,range} \approx 0.20$) for all three cases, with S3 being slightly larger, is found in the offshore area. At the end of the shoaling and in the outer breaking zone, an increase in wave-to-wave variability is observed for all three scenarios, with $Sk_{i,range} \approx 0.40$ for S1 and S2 and $Sk_{i,range} \approx 0.66$ for S3. In the latter case maximum values are $Sk_i = 1.11$ and minimum values are $Sk_i = 0.44$. The asymmetry in the offshore area is observed larger for S3 ($As_{i,range} \approx 0.40$), when compared to S1 and S2 ($As_{i,range} \approx 0.10$). However, the variability in asymmetry remains consistent throughout the outer breaking and inner surf zone, with the exception of S3 which reaches a maximum of $As_{i,range} \approx 0.73$. In the inner surf zone, wave-to-wave variability of both skewness and asymmetry reduces in all three scenarios, with corresponding ranges of $Sk_{i,range} \approx 0.07$and $As_{i,range} \approx 0.07$ for S1 and S2, $Sk_{i,range} \approx 0.25$and $As_{i,range} \approx 0.17$ for S3.

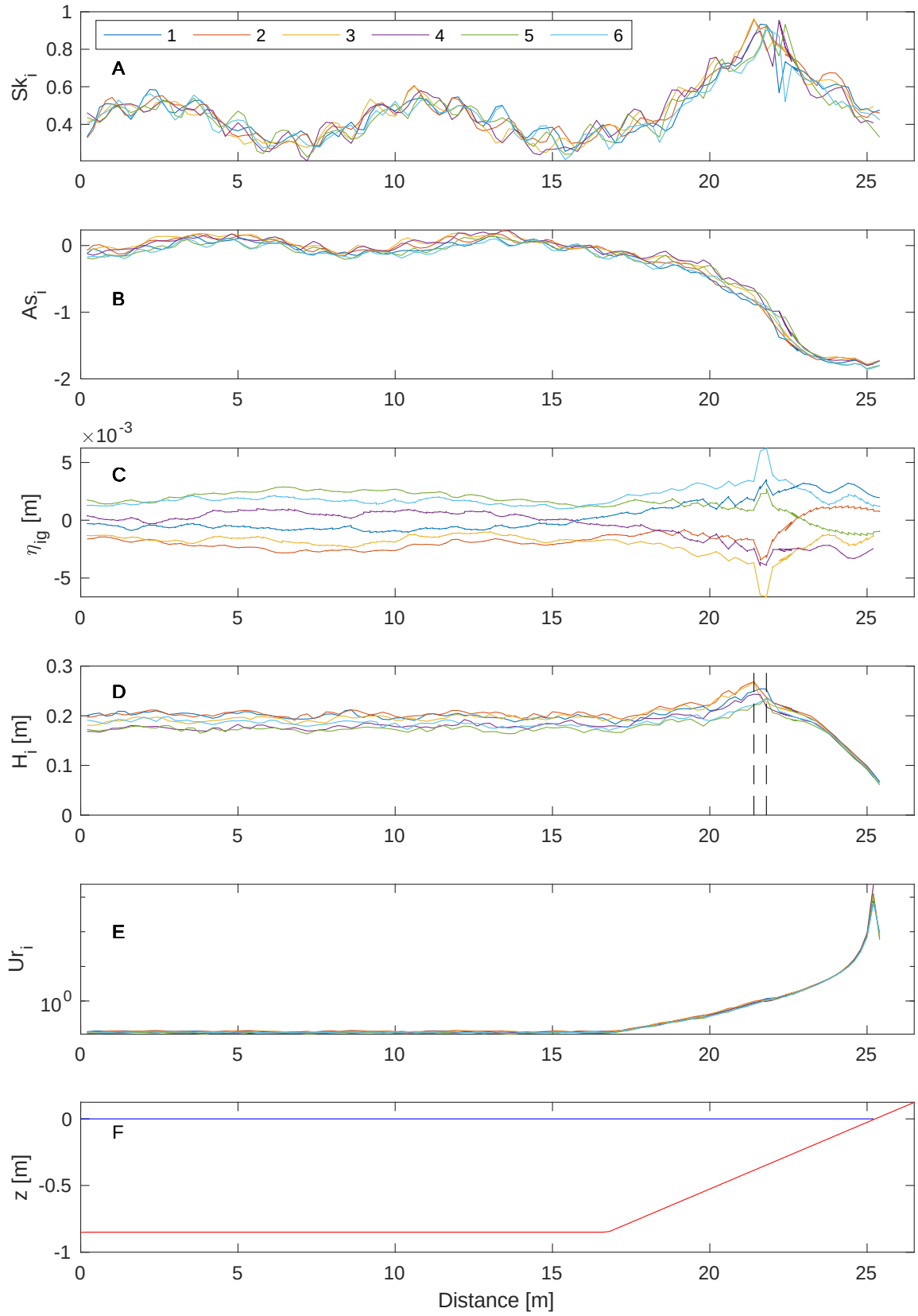

Figure 28: cross shore development for S1 of individual wave (a) skewness, (b) asymmetry, (c) infragravity wave induced mean water level offset, (d) height, (e) Ursell-number and (f) bottom contour (red) and still water level (blue)

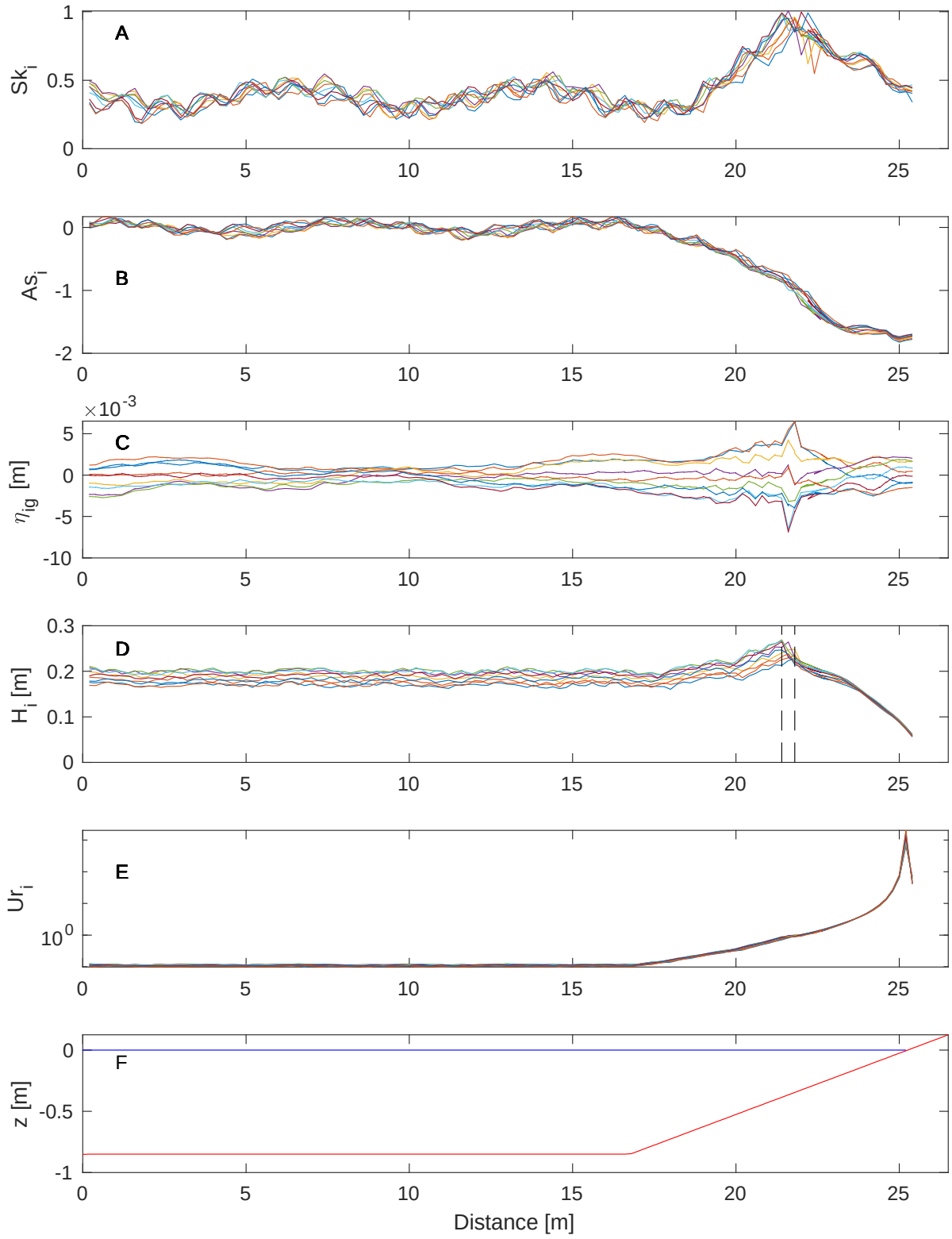

Figure 29: cross shore development for S2 of individual wave (a) skewness, (b) asymmetry, (c) infragravity wave induced mean water level offset, (d) height, (e) Ursell-number and (f) bottom contour (red) and still water level (blue)

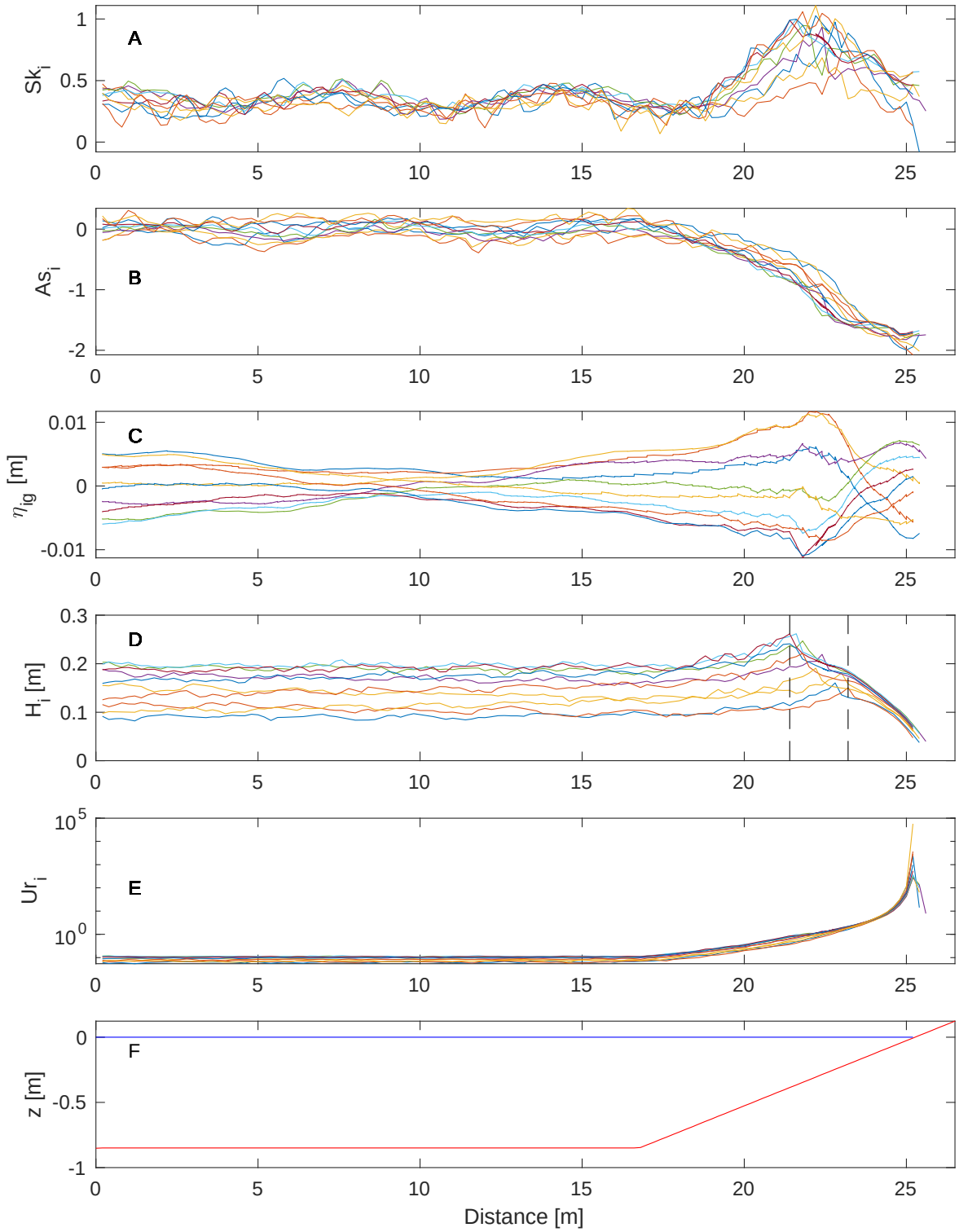

Figure 30: cross shore development for S3 of individual wave (a) skewness, (b) asymmetry, (c) infragravity wave induced mean water level offset, (d) height, (e) Ursell-number and (f) bottom contour (red) and still water level (blue)

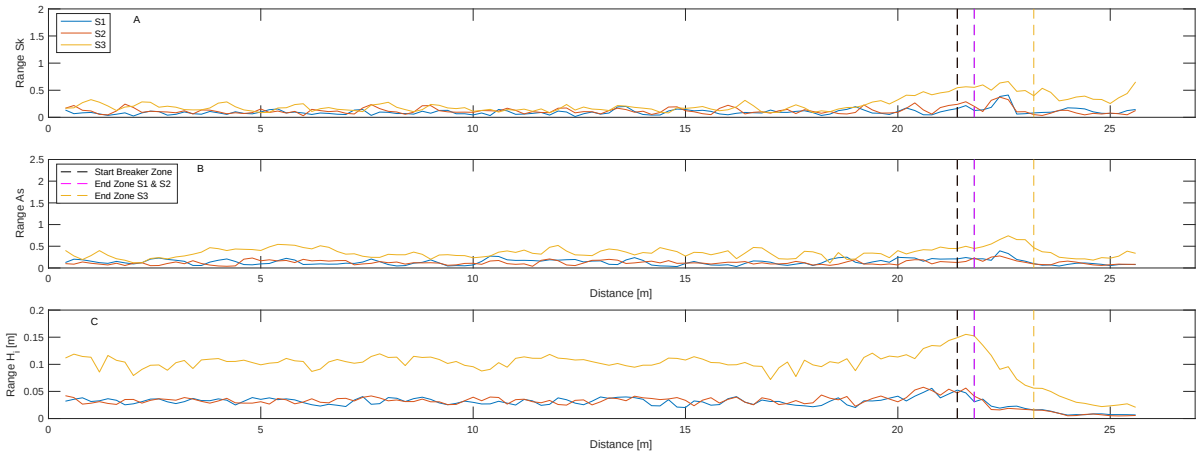

Figure 31: Development of range in individual (A) skewness, (B) asymmetry and (C) wave height (m), expressed as function of distance (m), for S1 (Blue line), for S2 (Red line) and S3 (Yellow line)

4.3 GLOBEX B3 vs. SWASH S3

As presented in the previous sections, series B3 and S3 demonstrate the strongest variability in all investigated wave characteristics. Figure 32 presents the results from individual wave tracking for experimental settings B3 and S3. As B3 is simulated over a gentle bed slope (1:80) and S3 over a steep bed slope (1:10), the total cross-shore distance over which the investigated area spans is different. For this reason, these characteristics are plotted as a function of depth (h) and both x- and y-limits have been set to similar values. This provides insight in the differences and similarities for the different bed slopes. It should be noted, that both cross-shore depth profiles contain a flat section, development over this area cannot be seen in Figure 32.

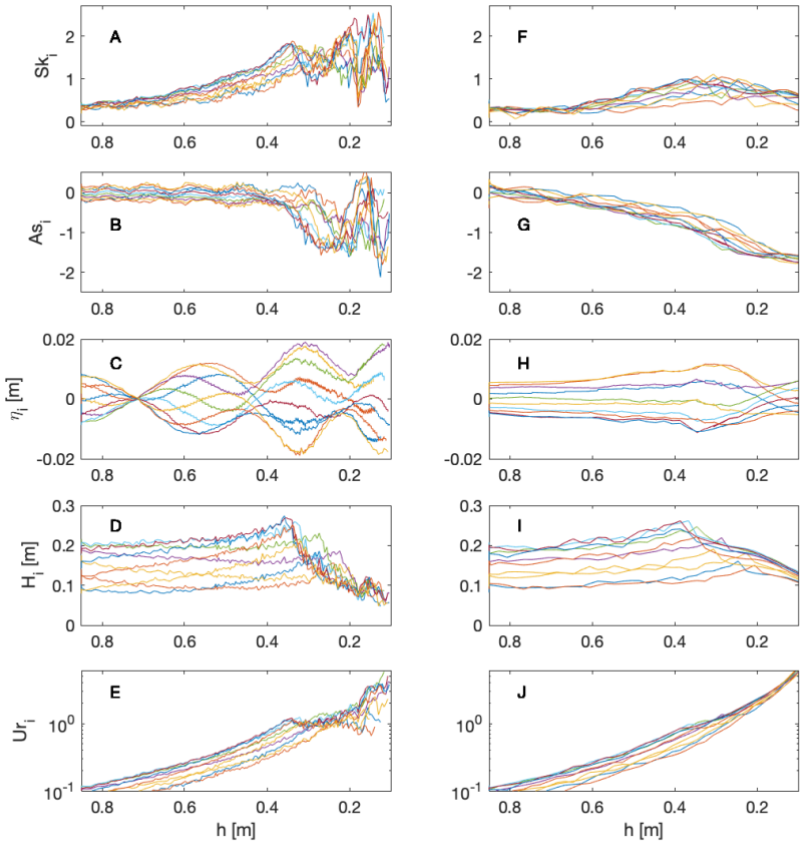

Figure 32: The cross-shore development of a single individual waves of one group from B3 (a) skewness, (b) asymmetry, (c) infragravity induced mean water level offset, (d) wave height, (e) Ursell-number; and for S3 (f) skewness, (g) asymmetry, (h) infragravity induced mean water level offset, (i) wave height, (j) Ursell-number.

The wave heights at the offshore depth ($h = 0.85\ m$) show a similar range, which is to be expected given the similar boundary wave conditions. As depths reduce over a longer distance for B3, individual wave heights are observed to alter more as

they propagate over the bed profile, some double in size (e.g. orange line $H_i = 0.123\,m$ at $h = 0.85\,m$ and $H_i = 0.247\,m$ at $h = 0.33\,m$). These alterations are not observed for S3. The development of the infragravity induced mean water level offset (Fig. 32C and 32H) shows that over a steep bed the infragravity waves has a less pronounced nodal structure (discussed in 4.2.1) and display less increase in amplitude. Interestingly, the range of depth over which the outer breaking zone spans is slightly larger for S3 (0.18 m), when compared to that of B3 (0.13 m). Also, wave breaking is initiated a larger depth for S3 at $h = 0.39\,m$. For B3, breaking is initiated at $h = 0.35\,m$.

The development of nonlinearity shows great differences for both cases. Firstly, at offshore depths, the skewness is fairly similar for B3 and S3, with $Sk_i \approx 0.3$. An increase in skewness is initiated for B3 in deeper water, at $h \approx 0.7\,m$. For S3 this increase is initiated around $h \approx 0.6\,m$. Towards the outer breaking zone, located at $h \approx 0.37\,m$, values for skewness are higher for B3, with $Sk_i \approx 1.3$. In the case of S3, the values for skewness average around $Sk_i \approx 0.7$. The wave-to-wave variability for both cases is comparable at $h = 0.37\,m$ with a range of $Sk_{i,range} \approx 0.7$. The opposite is observed for the development of asymmetry, which becomes more pronounced in deeper water for S3, when compared to B3. Notably, *As*-values reached as wave breaking is initiated, are comparable for both cases, with $As_i \approx -1.5$ at $h \approx -0.37\,m$. Theoretically, *As* values cannot be much smaller as this already equates to nearly vertical front faces of waves. However, for the case of B3, the range is larger at this same point ($As_{i,range} \approx 1.5$).

The largest differences are found in the inner surf zone. Here, strong wave-to-wave variability is observed for the individual development of skewness and asymmetry in the case of B3, especially around $h = 0.18\,m$, with ranges of $Sk_{i,range} \approx 1.6$ and $As_{i,range} \approx 1.8$. For S3 this is not the case; in the inner surf zone, individual waves show uniform behaviour with low wave-to-wave variability, with ranges of $Sk_{i,range} \approx 0.17$ and $As_{i,range} \approx 0.25$. This is much smaller when compared to B3. Notably, at $h = 0.18\,m$, the individual wave heights are smaller for B3, with $H_i \approx 0.07\,m$. At this same point for S3 individual wave heights average around $H_i = 0.15\,m$. With regards to Ursell, great resemblance between B3 and S3 is observed, up until depths where wave breaking is initiated. Within the outer breaking zone and the inner surf zone, strong variability is observed for B3, whilst *Ur*-values for S3 increase uniformly.

5. Discussion

This study set out to investigate the development of wave-to-wave variability of non-linearity in the cross shore (research question 1), assess the influence of bed slope on this variability (research question 2) and relate findings to the presence of infragravity waves (research question 3). The presented results allow for some preliminary conclusions to be drawn and further discussed, in order to come up with meaningful answers.

On a gentle bed (1:80), the variability of skewness increases throughout the shoaling zone, especially when wave groups are enhanced ($Sk_{i,range} = 0.75$), indicating that larger

differences in wave height account for larger differences in the development skewness. Close to and within the outer breaking zone, waves become increasingly asymmetric. Consequently, the wave-to-wave variability in asymmetry increases. To reiterate, when wave groups are enhanced this is especially prominent, maximum variability is reached in the outer breaking zone ($As_{i,range} = 1.52$). In the inner surf zone, independent from the boundary wave conditions, large wave-to-wave variability is observed ($Sk_{i,range}$ & $As_{i,range} \approx 1.6$). This is in accordance with findings by Tissier et al. (2015) regarding wave-to-wave variability in wave celerity.

On a steep bed (1:10) individual wave skewness is observed to be generally smaller than on a gentle bed. Individual wave asymmetry is initiated at greater depth, but reaches similar maximum negative values. This is in correspondence with findings by Rocha et al. (2017). The wave-to-wave variability in both skewness and asymmetry is observed to be smaller, when compared to variability on a gentle bed. As waves become increasingly skewed throughout the shoaling zone and increasingly asymmetric close to and within the outer breaking zone. A slight increase in variability is observed, only when wave groups were enhanced ($Sk_{i,range}$ & $As_{i,range} \approx 0.6$). The wave-to-wave variability reduces in the inner surf zone. On a gentle bed the wave-to-wave variability drastically increased in the inner surf zone.

In order to assess what drives the wave-to-wave variability, why it is generally smaller on an steep bed slope and if large variability in the inner surf zone on a gentle bed can be attributed to the presence of infragravity waves, the indivual wave observations for skewness and asymmetry are presented as a function of Ursell. Findings from the individual wave shape analyses are compared to fits suggested by Ruessink et al. (2012). Next, a comparison between the conventionally calculated non-linearity and the mean of individually tracked waves is made. This comparison provides insight in possible discrepancies and if these occur at locations where wave-to-wave variability is largest. What follows, is a reflection on the presented hypotheses based on previous studies. Finally, research uncertainties and limitations are discussed, followed by suggestions for future work.

5.1 Ursell-number and Ruessink (2012) Parameterisations

The Ursell-number is a parameter of wave nonlinearity and is commonly based on bulk estimates of wave statistical parameters, such as wave height and period, combined with water depth. In this study the Ursell number is computed for individual waves as a function of their wave height, period and local water depth, as described in section 3.2.4. Depth (h_i) was previously calculated including the infragravity induced mean water level offset and set-up and set-down. In order to isolate the influence of infragravity waves, the water level fluctuations the these waves induce have not been included in the variation of depth, used to calculate the Ursell-number in the following analysis. Thus, variability in Ur_i is only driven by the short wave characteristics. Findings are presented in Figure 34 (series B3) and 35 (series S3). A colour scale was added to each data point, describing the ratio between the

significant wave height of the infragravity wave ($H_{s,ig}$, calculated for the entire time series) and the local depth. This allows better insight in the influence of infragravity waves. $H_{s,ig}$ has been plotted as a fuction of depth (h) in Figure 33.

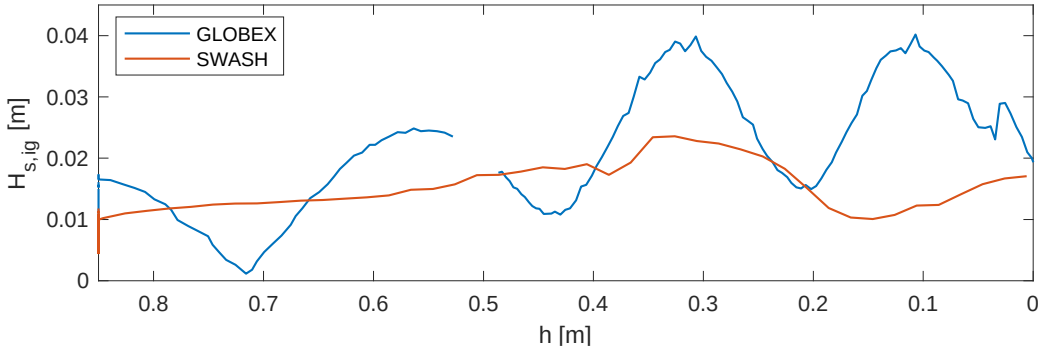

Figure 33: cross shore development of infragravity wave significant height (blue line) series B3 and (orange line) series S3, expressed as function of depth (m)

Ruessink et al. (2012) suggested a parameterisation for orbital velocity skewness and asymmetry, based on 30.000 + field observations, as a function of the Ursell-number. Values of skewness and asymmetry were combined into a measure of the total non-linearity *B* as a function of *Ur* (Eq. 13). The suggested fit was found using a Boltzman simoid combined with a non-linear least-squares fitting procedure, and for phase (ψ, Eq. 14) a *tanh*-function was used, resulting in the following:

$$B_{Ur} = p_1 \frac{p_2 - p_1}{1 + exp\frac{p_3 - \log(Ur)}{p_4}} \qquad \text{eq. 13}$$

$$\psi = -90° + 90° \tanh\left(\frac{p_5}{Ur^{p_6}}\right) \qquad \text{eq. 14}$$

With $p_1 = 0$, $p_2 = 0857$, $p_3 = -0.471$, $p_4 = 0.297$, $p_5 = 0.815$ and $p_6 = 0.672$. Skewness and asymmetry are computed from $Sk = Bcos\psi$ and $As = Bsin\psi$. It should be noted that this fit is based on the nonlinearity of the orbital velocity (Sk_u and As_u), which follows close patterns to the waveshape nonlinearity (Sk_η and As_η). Rocha et al. (2017) observed strong correlation of between Sk_u & As_u and Sk_η & As_η, indicating that the orbital velocity skewness and asymmetry are a direct reflection of wave shape skewness and asymmetry, although with smaller absolute values (40%). For each individually tracked wave at each time step, the skewness and asymmetry of waveshape are used to compute $B_{sk,as}$ using Equation 15:

$$B_{sk,as} = \sqrt{{Sk_{i,\eta}}^2 + {As_{i,n}}^2} \qquad \text{eq. 15}$$

Figure 34A shows the $B_{sk,as}$ (based on waveshape) plotted as a function of B_{Ur} (based on orbital velocity) for series B3. The red dotted line shows a 1/1 relation, which as expected shows large under estimation. As Rocha et al. (2017) observed this orbital velocity non-linearity to be 40% of the wave shape non-linearity, a 2.5/1 relation is plotted (blue line). This

demonstrated to more accurately describe the relation between B_{ur} and $B_{sk,as}$. Though a polynomial fit would have better suited, it shows that the estimation by Rocha et al. (2017) is of the correct order of magnitude.

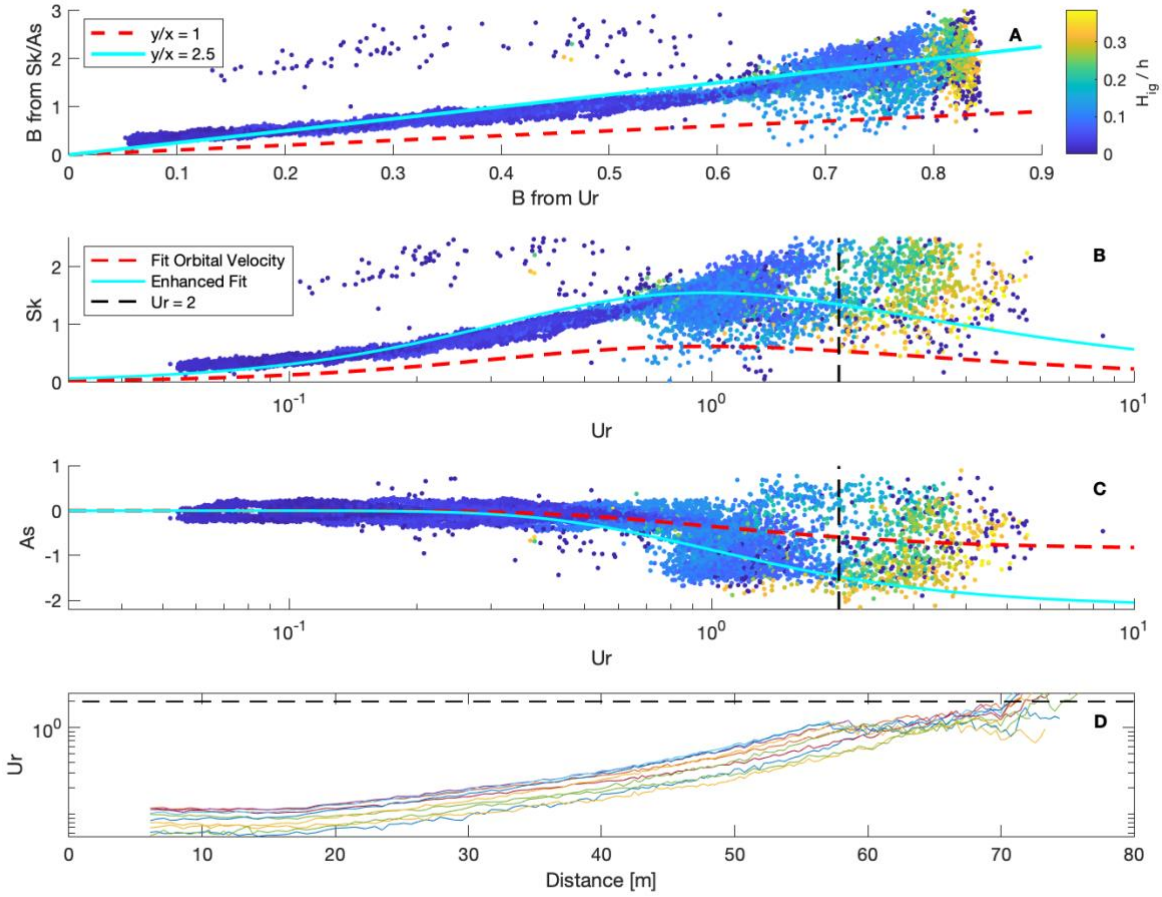

Figure 34: for series B3:(A) combined non-linearity parameter B based on wave shape (y-axis) as function of B based on Ur (x-axis); (B) skewness as function of Ur; (C) Asymmetry as function of Ur; (blue line) enhanced fit, (dashed line) 1:1 fit; colour code signifies the infragravity wave height to depth ratio; (D) individual cross shore development of Ur.

In Figure 34B and 34C the Ursell-number observations are plotted against the skewness and asymmetry observations as retrieved from the individual wave tracking, these are represented by the scattered dots. The fits as suggested by Ruessink et al. (2012,) are plotted in the red dashed line. As these fits describe orbital velocity, *B* was enhanced by a factor of 2.5 to better match the waveshape nonlinearity, plotted as the blue line. Apart from these fits being based on orbital velocity, the suggested fits are not based on skewness and asymmetry of individual waves, but on time averaged values for these parameters. I.e. the relation, as suggested by Ruessink et al. (2012), between Ursell-number and skewness and asymmetry does not capture the wave-to-wave variability in nonlinearity. When the individual Ursell-number and non-linearity of waveshape show similar trends to the Ruessink et al. (2012) fits this means that the short wave characteristics, used to calculate the individual Ursell (wave height and period) dominate the wave-to-wave variability in skewness and asymmetry. If the trend of the fits is not represented by the cloud of data points, this indicates

that short wave characteristics are not capable of explaining the wave-to-wave variability of skewness and asymmetry. This is discussed qualitatively.

For small Ursell-number values ($Ur < 1$) a clear trend is visible for both skewness (Fig. 34B) and asymmetry (Fig. 34C). This trend does not exactly follow the enhanced fit but could describe a clear relation with adjustment of the *p_x-coefficients*. With regards to *Sk* for low *Ur* (<1), a slight exponential growth is observed towards $Ur = 1$, where $Sk \approx 1.5$. Some outlier values are found, especially with regards to skewness. This is the result of inaccurate wave tracking. However, as 400,000+ data points are plotted, this is negligible. With regards to *As,* low *Ur* (<1) values describe a clear trend that remains around $As \approx 0$. When larger Ursell-number values are reached ($Ur > 1$) a much wider range of values for *Sk* and *As* is present. This range increases with increasing *Ur*. From Figure 34D, where the development of individual Ursell-number is plotted, it is evident that Ur_i is low a the offshore boundary ($Ur_i < 1$). This increases uniformly for the individual waves throughout the shoaling zone. At the initiation of breaking zone ($\mathrm{x} > 55\ \mathrm{m}$) intermeditate Ur_i is observed ($Ur_i \approx 1$). This implies that in the offshore and shoaling area, where Ur < 1, the short wave characteristics are capable of explaining the variability in *Sk* and *As*.

In the surf zone waves reduce in wave height, but as depths decrease Ur_i remains constant $Ur_i \approx 1$ or increase to values of $Ur_{max} \approx 4$. Dashed lines were plotted at $Ur_i = 2$ for reference. From Figure 34D, it becomes apparent that few waves reach values higher than this reference value, very far within the surf zone ($x > 70\ m$). In Figure 34B and 34C, for $Ur_i > 1$ much scatter of *Sk* and *As* is observed with no clear trend. This indicates that *Ur,* based individual short wave height, period and depth, is not capable of explaining variability in *Sk* and *As.* With regards to the influence of infragravity waves, a clear trend is visible in the colour scale added to the data points. Scatter is mostly caused by data points that where found with a higher ratio between significant infragravity wave height and depth (H_{ig} / h_i). This leads to believe that infragravity waves are possibly one of the driving factors behind the large wave-to-wave variability found in the inner surf zone.

Rocha et al. (2017) suggested that the bed slope has an influence on the relation between *Ur* and the non-linearity parameters as suggested by Ruessink (2012). This is observed in Figure 35A, where a total of 150,000+ data points retrieved from S3 are visualised. The 40% approximation appears to be a large overestimation in the case of a steep bed slope (1:10), confirming suggestions by Rocha et al. (2017). In Figure 35B and C a lion share of data points is located at low *Ur* values (< 0.1). This is a direct consequence of low *Ur* values identified from the offshore boundary up until $x = 17\ m$ (Fig. 35D). Despite over and under estimations of the (enhanced) fits (Ruessink et al., 2012) a similar trend is observed in the scatter, with max *Sk*-values at $Ur = 1$, and a negative trend for *As* with a steeper decrease around $Ur = 1$. This indicates, opposite to findings for B3, in the case of a steeper bed the variability in *Sk* and *As* is explained by the short wave characteristics (wave height and period) that make up the Ursell-number. This is also confirmed by the colour scale presented in Figure 35, where for larger *Ur*-values ($Ur > 1$), the ratio of H_{ig} / h_i was observed to be lower when compared to findings of B3 (Fig. 34).

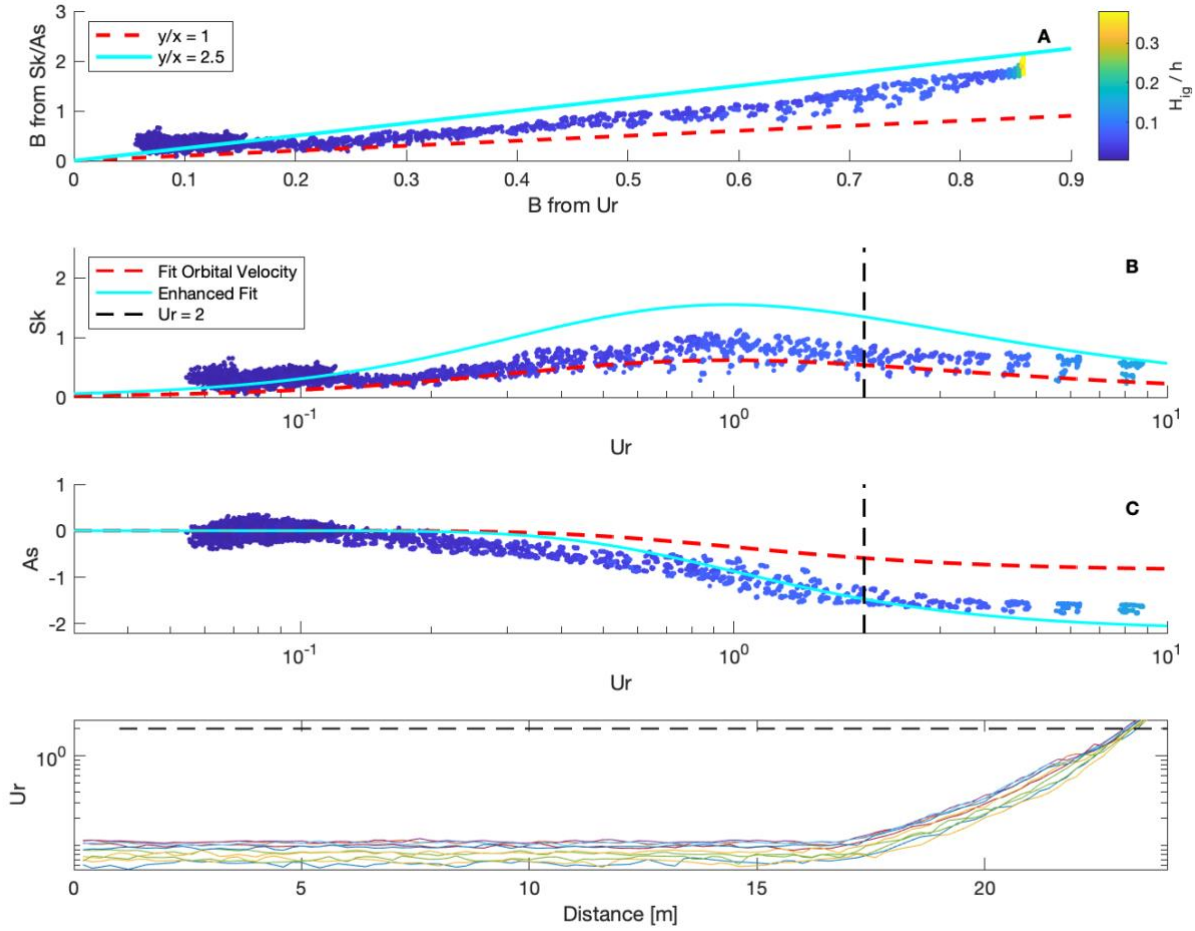

Figure 35: : for series S3:(A) combined non-linearity parameter B based on wave shape (y-axis) as function of B based on Ur (x-axis); (B) skewness as function of Ur; (C) Asymmetry as function of Ur; (blue line) enhanced fit, (dashed line) 1:1 fit; colour code signifies the infragravity wave height to depth ratio; (D) individual cross shore development of Ur.

As suggested by Abdelrahman and Thornton (1987), infragravity waves are capable of modulating short wave height and length. Tissier et al. (2015) found an increase of variability in celerity within the inner surf zone and related this to the presence of infragravity waves. De Bakker et al. (2016) showed that on a gentle bed slope, infragravity waves are more progressive and can become energetically dominant. Thus, infragravity waves can modulate short waves, whilst on a steep bed slope this effect is expected to be absent. Figure 36 shows the variance density of GLOBEX B3 and SWASH S3 in shallow water (Fig. 32A, h = 0.17 m; Fig 35B h = 0.14 m), both well within the inner surf zone. In series S3 the primary wave frequency (f_1) is found to be energetically dominant over the infragravity frequency (f_{ig}), with $f_1 = 0.436\, m^2/Hz$ and $f_{IG} = 0.004\, m^2/Hz$. In series B3 the infragravity wave frequency (f_{ig}) is found to be energetically dominant, with $f_1 = 0.014\, m^2/Hz$ compared to $f_{1,har} = 0.019\, m^2/Hz$.

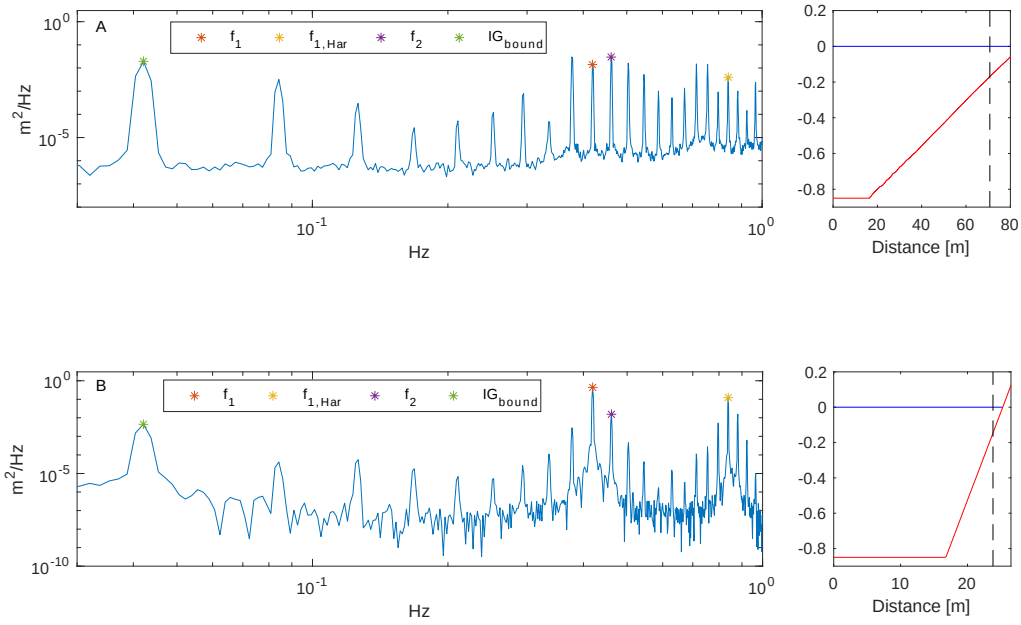

Figure 36: Variance density plot for (A) series B3 and (B) series S3, included on the right is the location where the frequency distribution was captured (dashed lines)

In summary, on a steep bed slope (1:10), clear relations between Ur_i and Sk_i & As_i are observed, without much scatter (Fig. 35). This indicates that *Ur* adequately explains the development of wave-to-wave variability in non-linearity. Short wave energy is found to be dominant in the inner surf zone (Fig. 36). This explains why *Ur,* computed as a function of short wave characteristics, adequately predicts non-linearity throughout the cross-shore, both in the shoaling and surf zone. On a steep bed, infragravity waves were not expected to modulate short waves, based on findings by De Bakker et al. (2016).

Based on field data, De Wit et al. (2019) found that the predicting capabilities of *Ur,* with regards to *Sk* and *As,* are less accurate and result in scatter in the surf zone. The individual wave analysis applied in this study observed similar behaviour, on a gentle bed slope. In the inner surf zone *Ur* (based on short wave characteristics) is not capable of explaining variability of skewness and asymmetry, especially at locations where H_{ig} / h_i is large. This indicates that infragravity does relate to the observed increase in wave-to-wave variability of non-linearity. This is backed by an energetic dominance of infragravity frequencies at shallower depths (Fig. 36). De Wit et al. (2019) appoint this increase in scatter (for $Ur > 1$) to complex hydrodynamics such as wave-breaking and the nonlinear energy transfer rate. Findings presented in this study hint at a possible relation between infragravity waves and an increase in the wave-to-wave variability of skewness and asymmetry in the inner surf zone.

As depths are small within the inner surf zone, it is evident that this is also the location where the ratio of H_{ig} / h_i is larger. For this reason, it should be noted that at the shallow locations where the complex hydrodynamic processes, as suggested by De Wit et al. (2019), are prominent, these are also the locations where inherently H_{ig} / h_i is larger. This means that the provided results cannot consolidate that this wave-to-wave variability in non-linearity is directly caused by the presence of infragravity waves. It is for this reason that further isolation

of the effects of the infragravity waves is suggested. This is more elaborately discussed in section 5.4.

5.2 Conventional vs. Mean of Individual Waves

As mentioned in the introduction, wave shape skewness and asymmetry have strong implications for sediment transport. Conventionally, skewness and asymmetry are computed over a total time series containing high frequency filtered free surface elevation for a limited number of gauges. The high-resolution datasets of GLOBEX and SWASH allowed for individual wave tracking and provided insight in wave-to-wave variability in non-linearity. It has been observed that wave-to-wave variability is large on a gentle bed slope, mainly in the inner surf zone (e.g. B3). Possible discrepancies were expected to occur here. In order to investigate whether this more detailed approach to assessing non-linearity indeed leads to discrepancies with the conventional approach, both conventionally calculated skewness and asymmetry have been plotted with the mean of the individual waves for the single assessed group (Fig. 37). In dashed lines the minimum and maximum values observed at each location have been plotted. Both cross-shore developments of non-linearity have been compared linearly for similarity and corresponding R^2-values and slope coefficients are presented in Table 3. The conventional non-linearity is computed using Equation 1 and 2 for entire time series. The mean of the individual wave tracking was computed using the following equations:

$$Sk_{x,mean} = \frac{1}{N} \sum_{i=1}^{N} Sk_{x,i} \qquad \text{eq. 16}$$

$$As_{x,mean} = \frac{1}{N} \sum_{i=1}^{N} As_{x,i} \qquad \text{eq. 17}$$

where N represents the number of waves making up a single wave group ($N = 6$ for B1 and S1; $N = 10$ for B2, B3, S2 and S3) and *x* represents the location of each gauge.

Table 3 and Figure 37 present that, the mean of individual waves and conventional non-linearity, generally show strong resemblance, with Slope Coefficients between 0.93 and 1.04; and R^2-values between 0.91 and 1.00 (with the exception of *Sk* B3). On a steep bed slope with small wave-to-wave variability, great similarity is observed. All slope coefficients are close to 1.00 (± 0.02). R^2-values are observed that > 0.99 for all three cases with regards to asymmetry, with regards to skewness, only S3 results in $R^2 = 0.92$. From Figure 37, it becomes apparent that only a minor discrepancy occurs at the most shoreward location, with a slight under estimation for the mean of individual waves. On a gentle bed, where wave-to-wave variability is generally larger, more pronounced discrepancies are found. Skewness in series B1 shows strong resemblance with an R^2 and the slope coefficient of 0.99. For B2, but mainly B3 show discrepancies. These occur mainly in the inner surf zone where wave-to-wave variability is largest. The conventionally computed skewness is lower than the mean skewness of individual waves. Asymmetry is observed to be slightly underestimated, in both B2 and B3,

by the conventional approach in the inner surf zone. Notably, the slope coefficients of B3 for both skewness and asymmetry are found to be lowest for all cases (Slope Coeff. = 0.93), with strong discrepancies in the inner surf zone. Here, this experimental setting showed strongest wave-to-wave variability for both skewness and asymmetry.

The mean of individual waves is considered in this analysis. However, it should be noted that it is not investigated whether individual waves, that show larger skewness or asymmetry have stronger implications for sediment transport. It could well be the case that this relation (as many other hydrodynamic processes) is non-linear. For example, if an individual skewness that is twice as large is observed, does this also mean it can transport twice the amount of sediment? This matter is to be more thoroughly assessed in future research, as it can generate better insight in the implications of individual wave skewness and asymmetry on sediment transport and, ultimately, geomorphology.

Table 3: R^2 and slope coefficients for linear comparison of conventionally computed non-linearity and non-linearity based on the mean of individually tracked waves

		B1	**B2**	**B3**	**S1**	**S2**	**S3**
Sk	R^2	0.99	0.95	0.84	0.99	0.99	0.92
	Slope Coeff.	0.99	1.01	0.93	1.00	1.01	0.98
As	R^2	0.98	0.93	0.91	1.00	1.00	0.99
	Slope Coeff.	1.04	0.94	0.93	1.02	1.02	0.98

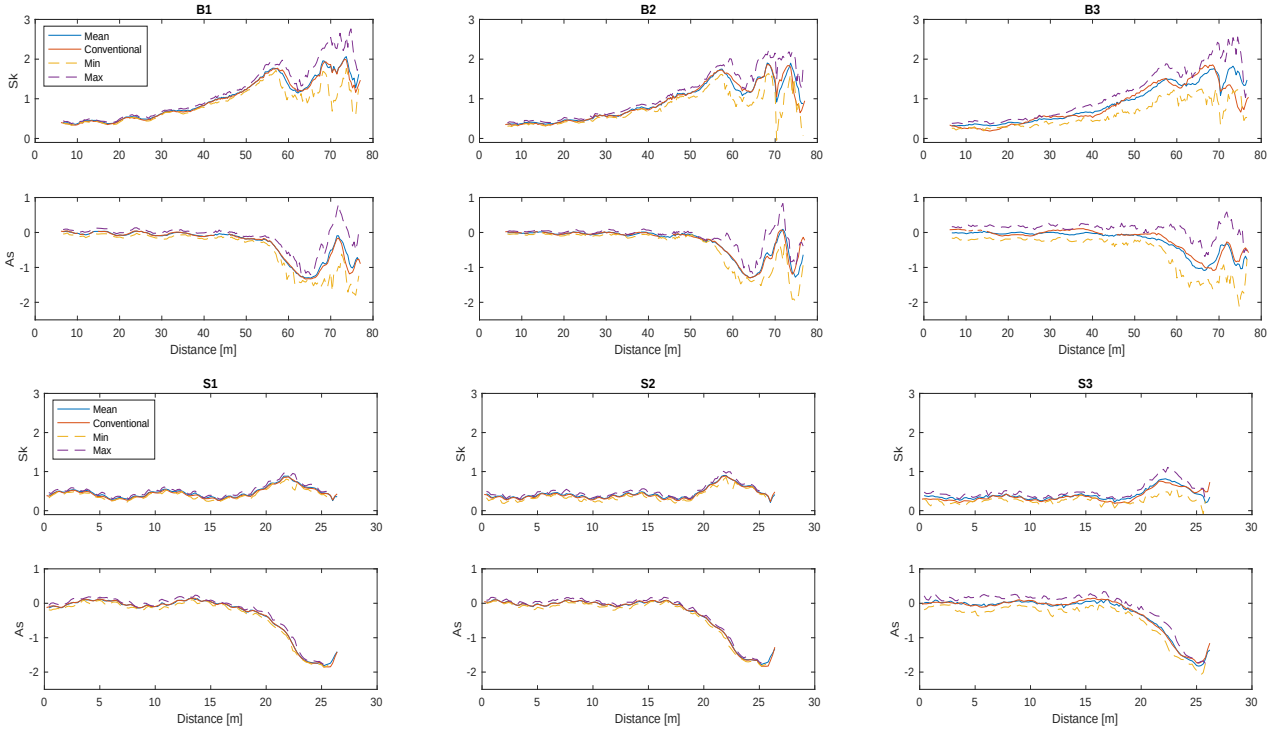

Figure 37: conventionally calculated non-linearity compared with the non-linearity as the defined by the mean of individually tracked waves (solid lines), maximum and minimum found at each location (dashed lines)

5.2 Reflecting on Hypotheses

Firstly, it was hypothesized from findings by Tissier et al. (2015) that individual waves show wave-to-wave variability in the development of skewness and asymmetry. This was found to be true. Figure 26 shows that, when wave groups are enhanced (GLOBEX series B3), indicating more pronounced differences between the largest and smallest waves of a group, wave-to-wave variability is generally larger. Based on findings by Rocha et al. (2017), it was expected that varying individual wave height would lead to an increase in variability of non-linearity, this has been confirmed. In section 5.1 an attempt was made at uncovering what drives wave-to-wave variability in non-linearity.

In the shoaling zone wave-to-wave variability in non-linearity was found to be driven by differences in short wave characteristics. Figure 34 shows the relation between skewness and asymmetry as predicted by the Ursell-number, which was calculated using individual short wave characteristics. For low *Ur* (<1), in deeper waters, a clear trend is observed, similar to those suggested by Ruessink et al. (2012). This indicates that short wave characteristics (e.g. wave height) are capable of explaining variation in non-linearity in the shoaling zone. This was expected on the basis of work by De Wit et al. (2019).

On a gentle bed (1:80), in the inner surf zone large variability for both skewness and asymmetry is observed ($Sk_{i,range}$ & $As_{i,range} \approx 1.6$ for B3). This was expected based on findings by Tissier et al. (2015) which indicated large variability in individual wave celerity in relation to infragravity waves at this location. This variability is also observed in Figure 34 for larger *Ur* (>1). This indicates that, within the inner surf zone, wave-to-wave variability is not explained by short wave characteristics. De Wit et al. (2019) observed similar behaviour and appointed this to complex hydrodynamics. Tissier et al. (2015) found that this increase in wave-to-wave variability in celerity occurs when infragravity wave height over depth ratio is large. By adding this ratio in colour scale to Figure 34, it is concluded that scatter in non-linearity occurs when $H_{ig}/h_i \geq 0.15$, indicating that infragravity waves are driving wave-to-wave variability. Notably, this is also the location where the complex hydrodynamics as suggested by De Wit et al. (2019), such as wave breaking and non-linear energy transfers, are important.

On a steep bed (1:10), in the inner surf zone low variability for both skewness and asymmetry is observed ($Sk_{i,range}$ & $As_{i,range} \approx 0.6$ for S3). This is reflected by the clear trend perceived in deeper water, which continues through the surf zone for larger *Ur* (>1). This indicates that in shallow water, wave-to-wave variability in non-linearity is still dominated by variability in the short wave characteristics. De Bakker et al. (2016) suggest that on a steep bed slope, as opposed to a gentle bed slope, infragravity waves are less progressive and modulation of short waves is absent. In this study, infragravity waves have indeed been observed to be less progressive (Fig. 30C) on a steep bed. This is also reflected in the infragravity wave height over depth ratio (H_{ig}/h_i, Fig. 35), which is low for high *Ur* (>1). This emphasises again that large wave-to-wave variability, observed in the inner surf zone on a gentle bed, is related to the presence of infragravity waves.

Section 5.2 indicates that, generally, the mean non-linearity of individually tracked waves shows great resemblance with conventionally calculated skewness and asymmetry. At locations where wave-to-wave variability increases, discrepancies are observed. This implies that, as a consequence of low variability of non-linearity found on a steep bed, great similarity in both ways of calculating non-linearity is observed. However, slight deviations occur in the most shoreward area, which are more pronounced when wave groups are enhanced. On a gentle bed, general trends are captured, but at locations where wave-to-wave variability is largest (in the inner surf zone), stronger discrepancies are found. These discrepancies are reflected in the slope coefficient and R^2.

5.4 Uncertainties and suggestions for future research

This research has compared laboratory-based information on free surface elevation of wave propagation over a gentle sloping bed, to modelled information of wave propagation on a steep sloping bed. Despite strong efforts and statistically satisfied tests on the correlation between the physical and modelled experiment, models will always remain a simplification of reality. Though general trends of the development of non-linearity are captured, with regards to skewness and asymmetry, wrong estimations were found in the validation runs (Fig. 21), with corresponding *R^2-values* of 0.73 for skewness and 0.61 for asymmetry. In the shoaling zone, trends between laboratory and modelled non-linearity show strong resemblance. Further shoreward ($x > 60\,m$), and especially in the surf zone, underestimations can be observed. Claims made in this study are largely based on the wave-to-wave variability observed in that location. In the surf zone, complex hydrodynamics play an important role, which possibly are not correctly predicted by SWASH. For future research it is suggested that both experimental settings would be executed physically, in order to add strength to claims made.

The benefit of models on the other hand, is that they are much more cost effective and less time consuming. This study has investigated two bed slopes: steep and gentle. For both slopes, it was found that the progressiveness of infragravity waves has implications for the development of variability in non-linearity within the surf zone. De Bakker et al. (2016) showed that this progressiveness is dependent on bed slope. Similar to Rocha et al. (2017), it is suggested for further research to simulate comparable experiments over a multitude of bed slopes, through modelling. By investigating wave-to-wave variability on varying bed slopes, possible trends could be identified.

As shown, the enhanced group modulation, as present in B3 and S3, increased the variability in non-linearity, mainly in the shoaling and breaking zone. In this study one type of boundary wave condition with enhanced group modulation has been studied. Similar to the proposition for including a multitude of bed slopes in a numerical modelling study, it would be interesting to also include a multitude of group enhancements.

The proposed wave tracking method worked well. However, as discussed in the inner surf zone ($x > 70\,m$), this became increasingly difficult. It is also here, were the effects of

the infragravity waves on variability in non-linearity of short waves was observed. The effects of the infragravity waves in GLOBEX become even more pronounced closer to shore and dominate swash motions completely (Ruessink et al., 2013). Due to time constraints, no waves were tracked by hand. This would have provided insight in processes in very shallow water that could have added to conclusions drawn in this study.

In this study wave-to-wave variability has been quantified as range. However, it is not said that this is the best representation of variability. Range is defined by the minimum and maximum non-linearity found at each location. This can be the result of one wave deviating greatly. For future research, it is suggested to also incorporate the standard deviation, as it better represents the common variation caused by all individual waves making up one wave group.

Finally, non-linearity of waves is studied thoroughly because of the implications this has on wave induced sediment transport. In this study, the variability of individual waves is discussed. However, it remains unclear if an individual wave, that shows twice the skewness when compared to another wave, also has twice the sediment transporting capabilities. A study to the relation of individual wave shape and individual wave transport could have even stronger implications for the use of parameterisations in morphodynamic models. Hopefully, this present work will serve as the basis of further research with regards to this.

6. Conclusion

This study is the first to track the development of skewness and asymmetry of individual waves. Its aim was to assess the development of variability of non-linearity in the cross-shore direction, by means of a data and modelling study. An individual wave tracking method was developed and has been applied to a dataset containing high resolution data (both in space and time) of bichromatic waves propagating over a low sloping bed (1:80), from the GLOBEX experiment. This laboratory dataset consisted of three different wave conditions, of which B3 consisted of waves with enhanced group modulation. The SWASH model has been utilised to recreate GLOBEX, in order to validate model settings and is ultimately used to simulate three similar wave conditions over a steep bed slope (1:10).

Three research questions have been defined in this study and will be answered here concisely, in order to sum up the main conclusions to be drawn from this present work.

Firstly, this study addresses *how the wave-to-wave variability of skewness and asymmetry develops in the cross-shore direction.* To summarize: on a gentle bed, in the shoaling zone, wave-to-wave variability is dominated by differences in short wave characteristics (e.g. wave height), thus is largest when wave groups are enhanced. This is concluded because the Ursell-number (based on short wave characteristics) was found to accurately predict non-linearity in this deeper area, where the influence of infragravity waves is low ($H_{ig}/h_i \leq 0.15$). Just before wave breaking is initiated, the range of variability in skewness reaches a local maximum ($Sk_{i,range} = 0.75$). In the outer breaking zone, wave-to-wave variability in

asymmetry is observed to reach its local maximum ($As_{i,range} = 1.52$). In the inner surf zone, large wave-to-wave variability in both skewness and asymmetry is observed, independent of the boundary wave conditions ($Sk_{i,range}$ & $As_{i,range} \approx 1.6$). Here, the Ursell-number was found to be unable to predict variation in skewness and asymmetry, with relation to a high infragravity wave height to depth ratio ($H_{ig}/h_i \geq 0.15$).

Secondly, this study aims to assess *the influence of bed slope on the wave-to-wave variability in nonlinearity.* On a steep bed slope, wave-to-wave variability was found to be smaller, when compared to a gentle bed slope. The range of both skewness and asymmetry was generally low. As waves become increasingly skewed throughout the shoaling zone, and asymmetric close to and within the outer breaking zone, a slight increase in variability is observed, only when wave groups were enhanced ($Sk_{i,range}$ & $As_{i,range} \approx 0.6$). In the inner surf zone, low wave-to-wave variability in non-linearity is observed. The Ursell-number is found to adequately explain non-linearity throughout the shoaling and surf zone. For higher *Ur*-values (>1), the infragravity wave height to depth ratio is observed to be lower than on a gentle bed slope ($H_{ig}/h_i < 0.15$).

Third and finally, this study investigated *the influence of the infragravity waves on wave-to-wave variability of non-linearity.* As mentioned in the previous paragraphs, there is a distinct difference in infragravity wave height to depth ratio between the gentle and steep bed slope found in the inner surf zone. This difference was observed to relate to a distinct increase in wave-to-wave variability within the inner surf zone. This leads to believe that, amongst other complex hydrodynamic processes, as found by De Wit et al. (2019), infragravity waves can influence the development of individual short wave non-linearity in the inner surf zone. It is suggested that further isolation of these near shore processes will be conducive to increasing the understanding of what drives wave-to-wave variability in non-linearity.

In a broader context, this detailed study after the development of individual waves has shed light on a tiny part of the complex hydrodynamic processes that drive our coastal systems. Hopefully, it will indirectly stimulate the implementation of sustainable solutions that protect our future coastal environment.

References

Abdelrahman, S. M., & Thornton, E. B. (1987). Changes in the short wave amplitude and wavenumber due to the presence of infragravity waves. In *Coastal Hydrodynamics* (pp. 458-478). ASCE.

Austin, M., Masselink, G., O'Hare, T., & Russell, P. (2009). Onshore sediment transport on a sandy beach under varied wave conditions: Flow velocity skewness, wave asymmetry or bed ventilation?. *Marine Geology*, *259*(1-4), 86-101.

Basco, D. R., & Yamashita, T. (1987). Toward a simple model of the wave breaking transition region in surf zones. In *Coastal Engineering 1986* (pp. 955-970).

Battjes, J. A. (1975). Surf similarity. In *Coastal Engineering 1974* (pp. 466-480).

Battjes, J. A., Bakkenes, H. J., Janssen, T. T., & van Dongeren, A. R. (2004). Shoaling of subharmonic gravity waves. *Journal of Geophysical Research: Oceans*, *109*(C2).

Battjes, J. A., & Janssen, J. P. F. M. (1978). Energy loss and set-up due to breaking of random waves. In *Coastal Engineering 1978* (pp. 569-587).

Bertin, X., De Bakker, A., Van Dongeren, A., Coco, G., André, G., Ardhuin, F., ... & Davidson, M. (2018). Infragravity waves: From driving mechanisms to impacts. *Earth-Science Reviews*, *177*, 774-799.

Bretschneider, C. L. (1959). *Wave variability and wave spectra for wind-generated gravity waves* (No. 118). The Board.

Brown, E. (1999). *Waves, tides and shallow-water processes* (Vol. 4). Gulf Professional Publishing.

Brown, S. (2011). Measures of shape: Skewness and kurtosis. *Retrieved on August*, *20*, 2012.

Benoit, K. (2011). Linear regression models with logarithmic transformations. *London School of Economics, London*, *22*(1), 23-36.

Chow, T. J., & Patterson, C. C. (1959). Lead isotopes in manganese nodules. *Geochimica et Cosmochimica Acta*, *17*(1-2), 21-31.

Doering, J. C., Elfrink, B., Hanes, D. M., & Ruessink, G. (2001). Parameterization of velocity skewness under waves and its effect on cross-shore sediment transport. In *Coastal Engineering 2000* (pp. 1383-1397).

Chai, T., & Draxler, R. R. (2014). Root mean square error (RMSE) or mean absolute error (MAE)?–Arguments against avoiding RMSE in the literature. *Geoscientific model development*, *7*(3), 1247-1250.

Crawford, W., Ballu, V., Bertin, X., & Karpytchev, M. (2015). The sources of deep ocean infragravity waves observed in the N orth A tlantic O cean. *Journal of Geophysical Research: Oceans*, *120*(7), 5120-5133.

Davies, A. G., & Li, Z. (1997). Modelling sediment transport beneath regular symmetrical and asymmetrical waves above a plane bed. *Continental Shelf Research*, *17*(5), 555-582.

de Bakker, A. T. M. (2016). *Infragravity-wave dynamics in shallow water: energy dissipation and role in sand suspension and transport* (Doctoral dissertation, Utrecht University).

Doering, J. C., & Bowen, A. J. (1987). Skewness in the nearshore zone: A comparison of estimates from Marsh-McBirney current meters and colocated pressure sensors. *Journal of Geophysical Research: Oceans*, *92*(C12), 13173-13183.

Doering, J. C., & Bowen, A. J. (1995). Parametrization of orbital velocity asymmetries of shoaling and breaking waves using bispectral analysis. *Coastal Engineering*, *26*(1-2), 15-33.

Elgar, S., & Guza, R. T. (1985). Observations of bispectra of shoaling surface gravity waves. *Journal of Fluid Mechanics*, *161*, 425-448.

Elgar, S., Guza, R. T., & Freilich, M. H. (1988). Eulerian measurements of horizontal accelerations in shoaling gravity waves. *Journal of Geophysical Research: Oceans*, *93*(C8), 9261-9269.

Galvin Jr, C. J. (1968). Breaker type classification on three laboratory beaches. *Journal of geophysical research*, *73*(12), 3651-3659.

Guza, R. T., & Thornton, E. B. (1982). Swash oscillations on a natural beach. *Journal of Geophysical Research: Oceans*, *87*(C1), 483-491.

Holthuijsen, L. H. (2010). *Waves in oceanic and coastal waters*. Cambridge university press.

Hughes, S. A. (1993). *Physical models and laboratory techniques in coastal engineering* (Vol. 7). World Scientific.

King, B. A., Blackley, M. W. L., Carr, A. P., & Hardcastle, P. J. (1990). Observations of wave-induced set-up on a natural beach. *Journal of Geophysical Research: Oceans*, *95*(C12), 22289-22297.

Longuet-Higgins, M. S., & Stewart, R. W. (1962). Radiation stress and mass transport in gravity waves, with application to 'surf beats'. *Journal of Fluid Mechanics*, *13*(4), 481-504.

Masselink, G., & Hughes, M. G. (2003). *Introduction to Coastal Geomorphology and Processes*.

Meyer, R. E. (Ed.). (2013). *Waves on Beaches and Resulting Sediment Transport: Proceedings of an Advanced Seminar, Conducted by the Mathematics Research Center, the University of Wisconsin, and the Coastal Engineering Research Center, US Army, at Madison, October 11–13, 1971* (Vol. 28). Elsevier.

Peregrine, D. H. (1967). Long waves on a beach. *Journal of fluid mechanics*, *27*(4), 815-827.

Ribberink, J. S., van der Werf, J. J., O'Donoghue, T., & Hassan, W. N. M. (2008). Sand motion induced by oscillatory flows: Sheet flow and vortex ripples. *Journal of Turbulence*, (9), N20.

Rocha, M. V. L., Michallet, H., & Silva, P. A. (2017). Improving the parameterization of wave nonlinearities–The importance of wave steepness, spectral bandwidth and beach slope. *Coastal Engineering*, *121*, 77-89.

Rijnsdorp, D. P., Smit, P. B., & Zijlema, M. (2014). Non-hydrostatic modelling of infragravity waves under laboratory conditions. *Coastal Engineering*, *85*, 30-42.

Ruessink, B. G., Kleinhans, M. G., & Van den Beukel, P. G. L. (1998). Observations of swash under highly dissipative conditions. *Journal of Geophysical Research: Oceans*, *103*(C2), 3111-3118.

Ruessink, B. G., Michallet, H., Bonneton, P., Mouazé, D., Lara, J., Silva, P. A., & Wellens, P. (2013). Globex: wave dynamics on a gently sloping laboraty beach. *Proceedings Coastal Dynamics 2013*, 1351-1362.

Ruessink, B. G., Ramaekers, G., & Van Rijn, L. C. (2012). On the parameterization of the free-stream non-linear wave orbital motion in nearshore morphodynamic models. *Coastal Engineering*, *65*, 56-63.

Schäffer, H. A. (1996). Second-order wavemaker theory for irregular waves. *Ocean Engineering*, *23*(1), 47-88.

Severance Jr, R. W. (1975). Optimum filtering and smoothing of buoy wave data. *Journal of Hydronautics*, *9*(2), 69-74.

Smit, P., Zijlema, M., & Stelling, G. (2013). Depth-induced wave breaking in a non-hydrostatic, near-shore wave model. *Coastal Engineering*, *76*, 1-16.

Symonds, G., Huntley, D. A., & Bowen, A. J. (1982). Two-dimensional surf beat: Long wave generation by a time-varying breakpoint. *Journal of Geophysical Research: Oceans*, *87*(C1), 492-498.

Van Rijn, L. C. (1990). *Principles of fluid flow and surface waves in rivers, estuaries, seas and oceans* (Vol. 12). Amsterdam, The Netherlands: Aqua Publications.

van Rijn, L., Ruessink, G., Grasmeijer, B., van der Werf, J., & Ribberink, J. (2007). Wave-related transport and nearshore morphology. In *Coastal Sediments' 07* (pp. 1-14).

Tissier, M., Bonneton, P., Michallet, H., & Ruessink, B. G. (2015). Infragravity-wave modulation of short-wave celerity in the surf zone. *Journal of Geophysical Research: Oceans*, *120*(10), 6799-6814.

TU Delft: SWASH. (n.d.). Retrieved from https://www.tudelft.nl/en/ceg/about-faculty/departments/hydraulic-engineering/sections/environmental-fluid-mechanics/research/swash/

Ursell, F. (1953, October). The long-wave paradox in the theory of gravity waves. In *Mathematical Proceedings of the Cambridge Philosophical Society* (Vol. 49, No. 4, pp. 685-694). Cambridge University Press.

Watson, G., Barnes, T. C. D., & Peregrine, D. H. (1995). The generation of low-frequency waves by a single wave group incident on a beach. In *Coastal Engineering 1994* (pp. 776-790).

Wunk, W. H. (1949). Surf beats. *EOS, Transactions American Geophysical Union*, *30*(6), 849-854.

Appendix

The following figures show that in different experimental settings, the same wave of the same groups acts exactly the same. Results from B1, B3 and S3 are presented here.

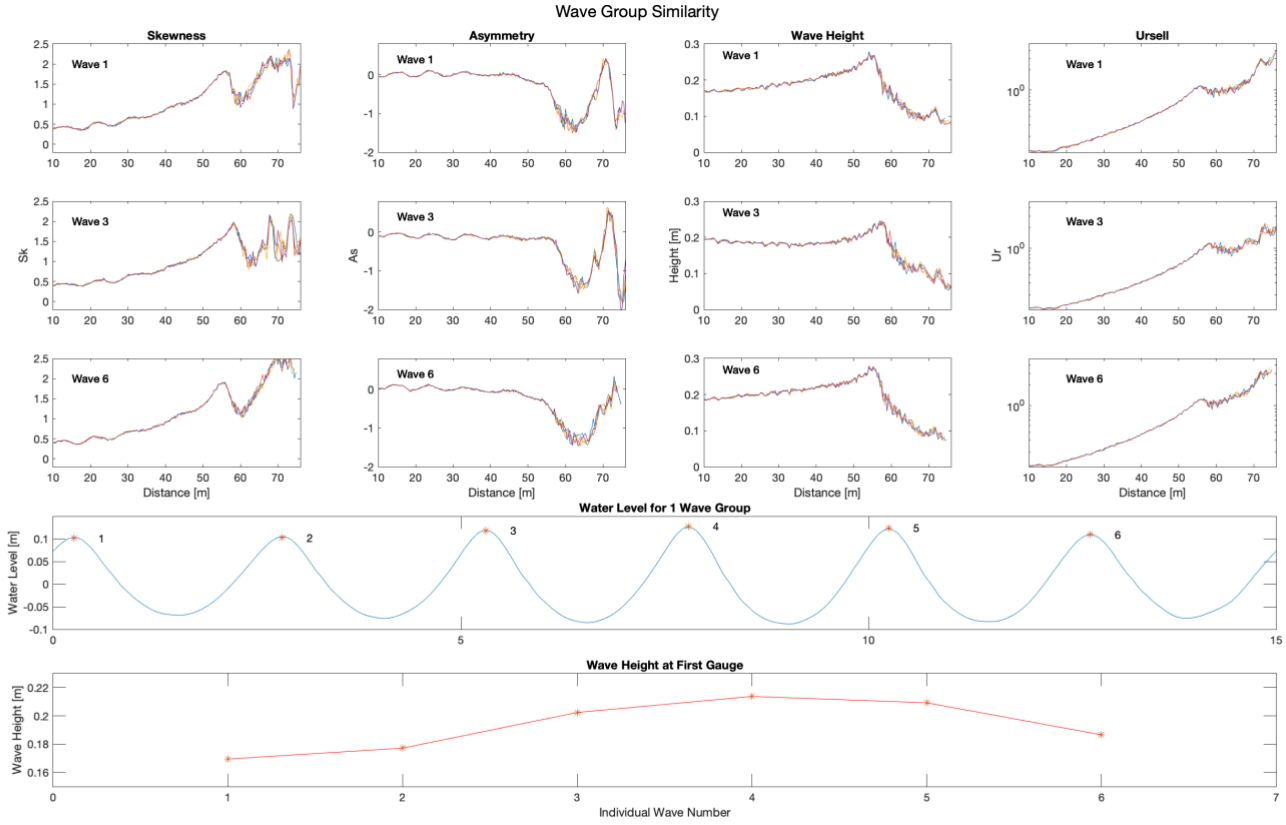

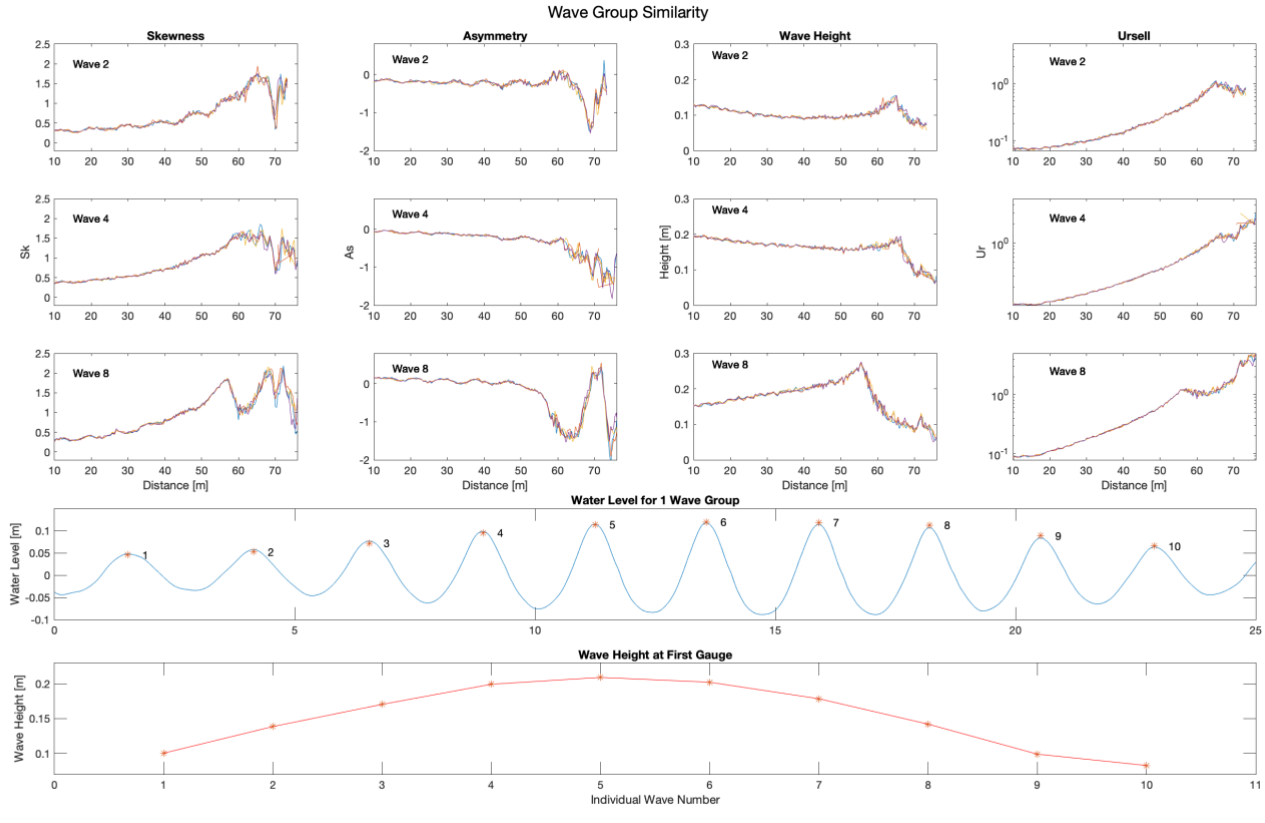

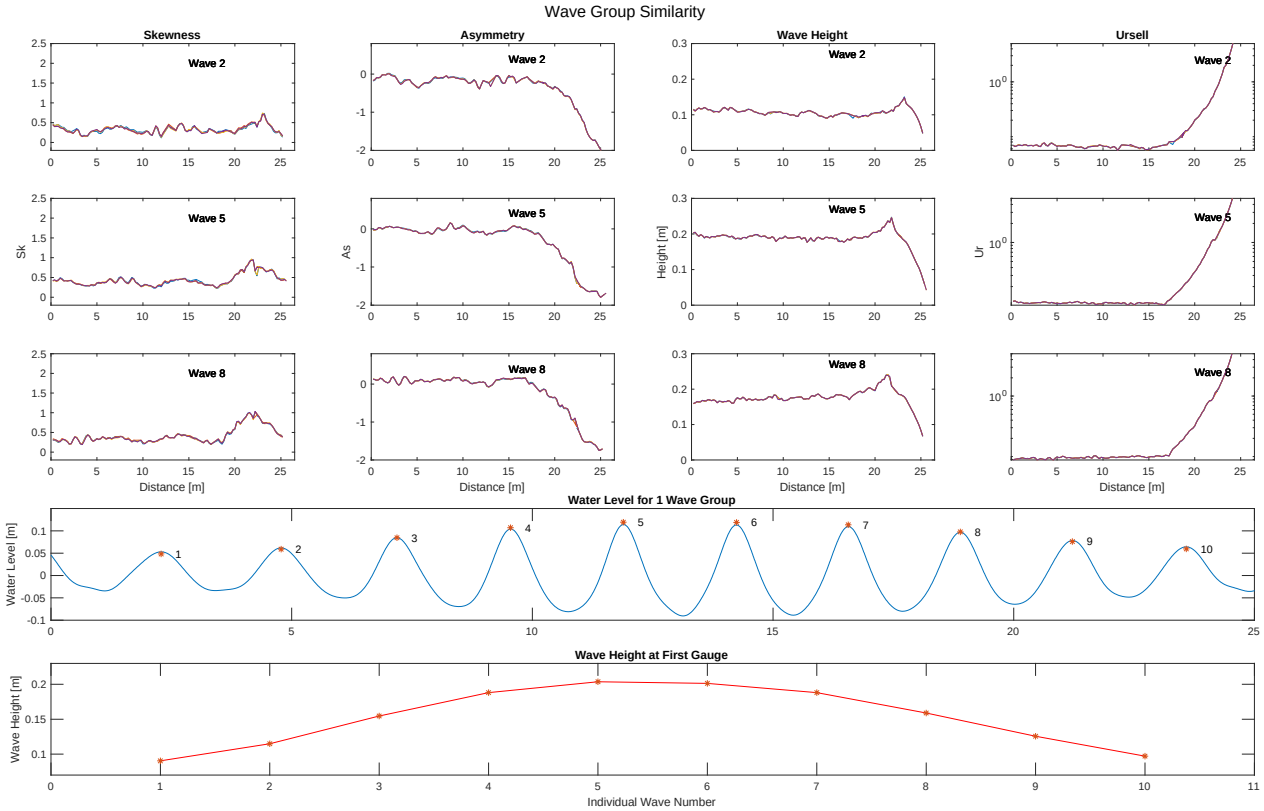

Figure 37, 38 & 39: For B1, B3 and S3; (a) similar development of individual waves from five different wave groups with label 2 (1st row), label 5 (2nd row) and label 8 (3rd row) for Sk (1st column), As (2nd column), H_i (3rd column) and Ur (4th column) as function of distance (m) ; (b) free surface elevation at the first gauge with corresponding wave label; (c) individual wave height at the first gauge plotted as function of wave label.